Published in final edited form as:
Neurobiol Dis. 2013 December ; 60: . doi:10.1016/j.nbd.2013.08.009.

Loss of Corticostriatal and Thalamostriatal Synaptic Terminals Precedes Striatal Projection Neuron Pathology in Heterozygous Q140 Huntington's Disease Mice

Y.P. Deng, **T. Wong**, **C. Bricker-Anthony**, **B. Deng**, and **A. Reiner**
Department of Anatomy and Neurobiology, The University of Tennessee Health Science Center, Memphis, TN 38163

Abstract

Motor slowing, forebrain white matter loss, and striatal shrinkage have been reported in premanifest Huntington's disease (HD) prior to overt striatal neuron loss. We carried out detailed LM and EM studies in a genetically precise HD mimic, heterozygous Q140 HD knock-in mice, to examine the possibility that loss of corticostriatal and thalamostriatal terminals prior to striatal neuron loss underlies these premanifest HD abnormalities. In our studies, we used VGLUT1 and VGLUT2 immunolabeling to detect corticostriatal and thalamostriatal (respectively) terminals in dorsolateral (motor) striatum over the first year of life, prior to striatal projection neuron pathology. VGLUT1+ axospinous corticostriatal terminals represented about 55% of all excitatory terminals in striatum, and VGLUT2+ axospinous thalamostriatal terminals represented about 35%, with VGLUT1+ and VGLUT2+ axodendritic terminals accounting for the remainder. In Q140 mice, a significant 40% shortfall in VGLUT2+ axodendritic thalamostriatal terminals and a 20% shortfall in axospinous thalamostriatal terminals was already observed at 1 month of age, but VGLUT1+ terminals were normal in abundance. The 20% deficiency in VGLUT2+ thalamostriatal axospinous terminals persisted at 4 and 12 months in Q140 mice, and an additional 30% loss of VGLUT1+ corticostriatal terminals was observed at 12 months. The early and persistent deficiency in thalamostriatal axospinous terminals in Q140 mice may reflect a development defect, and the impoverishment of this excitatory drive to striatum may help explain early motor defects in Q140 mice and in premanifest HD. The loss of corticostriatal terminals at 1 year in Q140 mice is consistent with prior evidence from other mouse models of corticostriatal disconnection early during progression, and can explain both the measurable bradykinesia and striatal white matter loss in late premanifest HD.

Keywords

Huntington's Disease; Corticostriatal; Thalamostriatal; Premanifest; Pathology

Address all correspondence to: Dr. Anton Reiner, Ph.D., Dept. of Anatomy and Neurobiology, The University of Tennessee Health Science Center, 855 Monroe Ave., Memphis, TN 38163, Phone: 901-448-8298, Fax: 901-448-7193, areiner@uthsc.edu.

The authors have no financial interest in the research reported here.

Introduction

Although considerable attention has focused on the role of differential striatal projection neuron loss in the progression of HD motor symptoms (Deng et al., 2004; Glass et al., 2000; Reiner et al., 1988; Richfield et al., 1995), little attention has focused on the neuronal pathology underlying the emerging motor symptoms reported in premanifest HD individuals. For example, numerous studies have noted that premanifest HD individuals are slowed in the initiation and/or execution of a variety of motor tasks involving the eyes, hands or lower limbs (Bechtel et al., 2010; Biglan et al., 2009; Blekher et al., 2004; de Boo et al., 1997; Delval et al., 2011; Kirkwood et al., 1999, 2000; Rao et al., 2008, 2011; Siemers et al., 1996; Tabrizi et al., 2011; Turner et al., 2011). This defect is mild in premanifest cases not yet near clinical onset, but more severe in those near onset (Bechtel et al., 2010; Kirkwood et al., 2000; Rao et al., 2008, 2011; Rupp et al., 2010). Diverse types of imaging studies (computed tomography, magnetic resonance imaging, positron emission tomography, and diffusion tensor imaging) show that these growing motor symptoms in premanifest HD occur in parallel with a slowly progressive loss of cerebral and striatal white matter (Aylward et al., 2011; Ciarmiello et al., 2006; Dumas et al., 2012; Hobbs et al., 2010a; Kipps et al., 2005; Paulsen et al., 2006; Reading et al., 2005; Rosas et al., 2006), striatal hypometabolism (Ciarmiello et al., 2006; Grafton et al., 1992), and reduced striatal activation during behavioral tasks (Paulsen et al., 2004; Wolf et al., 2012). Nonetheless, the limited neuropathological studies of premanifest striatum have reported little or no neuronal loss, particularly in the motor striatum (i.e. putamen) (Albin et al., 1991; Vonsattel et al., 1985; Vonsattel and DiFiglia, 1998).

These findings in premanifest human HD raise the possibility that the very earliest motor defects in HD victims may be related to the loss of afferent connectivity of motor striatum with its major sources of excitatory input – cerebral cortex and thalamus. Both inputs mainly end as terminals that make asymmetric synaptic contact with dendritic spines of striatal projection neurons, which make up the vast majority of striatal neurons (Albin et al., 1989; Gerfen, 1992; Reiner and Anderson, 1990; Smith et al., 2004; Wilson et al., 1982). The input from cerebral cortex, which arises from all cortical regions to a greater or lesser extent, is the more substantial of the two, and is thought to provide striatum with an instructive signal for its role in motor control (Gerfen, 1992, Wilson, 1992). The thalamic input, which arises heavily from intralaminar, mediodorsal and midline thalamic nuclei (Berendse and Groenewegen, 1990; Groenewegen and Berendse, 1994), however, also provides drive to striatum that is critical to its role in movement selection and facilitation (Kato et al., 2011; Smith et al., 2004, 2009, 2011). In symptomatic HD, neuronal loss occurs in cortical layers 3, 5, and 6, and is prominent by grade 4 (Byers et al., 1973; Cudkowicz and Kowall, 1990; De La Monte et al., 1988; Passani et al., 1997; Selemon et al., 2004; Sotrel et al., 1991; Vonsattel et al., 1985). Similarly, more than 50% neuronal loss in the intralaminar nuclei has been reported for advanced HD (Heinsen et al., 1996), and thalamic shrinkage in HD correlates with cognitive decline (Kassubek et al., 2004a,b). Consistent with their vulnerability in symptomatic HD, regional cortical thinning and volume loss, and thalamic volume loss have been seen in premanifest HD (Aylward et al., 2011; Rosas et al., 2005), although again without evidence of neuron loss (Vonsattel et al., 1985).

Thus, although available data suggest that early loss of excitatory cortical and/or thalamic input could be a major contributor to the striatal hypoactivity and motor abnormalities seen in premanifest HD, direct neuropathological evidence for such input loss is lacking. However, given the difficulties in obtaining EM grade fixation in human brain tissue and given the difficulty in obtain premanifest HD brains for neuropathological study, it would be challenging to address this issue by detailed EM study of human striatum. As an alternative approach, we examined thalamostriatal and corticostriatal input loss over the first year of

life in a precise genetic mimic of human HD, the heterozygous Q140 knock-in mouse, in which expression of the mutant protein occurs from the native gene (Hickey et al., 2008). Although homozygous Q140 mice show motor and behavioral abnormalities beginning by 6 months of age, and HD-like striatal neurochemical abnormalities and neuron loss by 12 months, the behavioral phenotype in heterozygous Q140 mice is more attenuated and mice are not yet overtly symptomatic at 1 year of age (Rising et al., 2011). To identify corticostriatal and thalamostriatal terminals in Q140 heterozygotes, we used immunolabeling for VGLUT1 and VGLUT2, respectively. Excitatory thalamic projection neurons use the vesicular glutamate transporter VGLUT2 for packaging glutamate in synaptic vesicles, while excitatory cortical neurons use VGLUT1 (Fremeau et al., 2001, 2004; Fujiyama et al., 2004; Herzog et al., 2001; Lei et al., 2013; Varoqui et al., 2002). We confirmed the absence of striatal pathology at 12 months in Q140 heterozygotes. Our results indicate deficiencies in thalamic input to the spines and dendrites of striatal neurons already at one month, with substantial loss of cortical input to the spines of striatal neurons evident at 1 year. Our results suggest that loss of thalamostriatal and corticostriatal terminals may, in fact, underlie motor impairments in premanifest HD.

Materials and Methods

Animals

Results from 35 WT and heterozygous Q140 mice (obtained from JAX, Bar Harbor, Maine) are presented here, and all animal use was carried out in accordance with the National Institutes of Health Guide for Care and Use of Laboratory Animals, Society for Neuroscience Guidelines, and University of Tennessee Health Science Center Guidelines. Heterozygous HD mutants were studied because the human disease most commonly occurs due to a single allelic defect. It should be noted that the repeat length in the Q140 mice that we used had undergone a spontaneous reduction during breeding at JAX, and the average repeat length in our eight 1-month old Q140 mice was 127.8, our five 4-month old Q140 mice was 128.6, and our five 12-month old Q140 mice was 135.0. Seven 1-month old WT mice, five 4-month old WT mice, and five 12-month WT mice were studied. For histological analysis, mice were deeply anesthetized with 0.2ml of 35% chloral hydrate in saline, and then exsanguinated by transcardial perfusion with 30 ml of 6% dextran in sodium phosphate buffer (PB), followed by 200 ml of 3.5% paraformaldehyde - 0.6% glutaraldehyde - 15% saturated picric acid in PB (pH 7.4). The brain of each mouse was removed, postfixed overnight in 3.5% paraformaldehyde - 15% saturated picric acid in PB. The right side of the brain was used for light microscopic (LM) and the left for electron microscopic (EM) analysis. For LM studies, forebrain was section at 35μm and collected as 12 parallel series, #1 and #7 of which were mounted on slides at the time for cresyl violet staining. For EM studies, forebrain was sectioned at 50μm on a vibratome.

Light Microscopic Visualization of VGLUT

Single-label immunofluorescence was carried out to examine the localization of VGLUT1 and VGLUT2 in striatal axons and terminals. For these studies, we used either a guinea pig VGLUT2 antibody (AB5907, Chemicon Temecula, CA) or a rabbit VGLUT2 antibody (V2514, Sigma), and a guinea pig VGLUT1 antibody (AB5905, Chemicon Temecula, CA). Sections were incubated overnight at room temperature either in the guinea pig anti-VGLUT2 (1:1000), rabbit anti-VGLUT2 (1:2000), or guinea pig anti-VGLUT1 (1:1000). After incubation in primary antibody at room temperature with gentle agitation, the tissue was rinsed three times, and the secondary antibody incubation carried out. The sections were incubated for 2 hours at room temperature (with gentle agitation) in an Alexa 594-conjugated goat anti-guinea pig IgG (to detect the guinea pig anti-VGLUT1 or guinea pig anti-VGLUT2) or an Alexa 594-conjugated goat anti-rabbit IgG (to detect the rabbit anti-

VGLUT2). Secondaries were from Molecular Probes (Eugene, OR), and were diluted at 1:200. Sections were rinsed three times in 0.1M PB after incubation in secondaries, mounted on gelatin-coated slides, and coverslipped with ProLong® antifade medium (Molecular Probes, Eugene, OR). Sections were viewed and images captured using a Nikon D-Eclipse C1 confocal laser scanning microscope (CLSM), using a 40× oil objective. Z-stack serial images were collected at 1μm (40× oil) steps from dorsolateral striatum. Note that some single-label tissue was also prepared using the peroxidase-antiperoxidase method as detailed in prior studies (Deng et al., 2006, 2007). Three striatal images from each of 3 sections at the level of the anterior commissure for each mouse were analyzed (thus totaling nine images per mouse) using the public-domain software NIH ImageJ (http://rsbweb.hih.gov/ij/download.html). For each image, five areas were selected for detailed measurement, four from each image quadrant and one from the center. Areas selected for measurement were 300–500 μm^2 in size, and free of perikarya or fiber bundles. Three types of measurements were made: 1) the mean labeling intensity of the selected area; 2) the intensity of the immunolabeled fibers in the selected area; and 3) the percent of the selected area covered by immunolabeled fibers. Immunolabeled fibers were highlighted by auto-thresholding to allow their selective measurement.

Light Microscopic Visualization of Striatal Neuron Markers

LM immunohistochemical analysis was carried out to determine the effects of the Q140 mutation on the neurochemical integrity of striatal projection neurons, as evaluated by their outputs to their target areas. The peroxidase-antiperoxidase (PAP) procedure as described previously (Reiner et al., 2007, 2012a) was used for substance P (SP) immunolabeling to study SP+ striatal projection systems, and for enkephalin (ENK) immunolabeling to study ENK+ striatal projection systems. The anti-SP was a rabbit polyclonal antibody (ImmunoStar, Hudson, WI) whose specificity has been documented previously (Figueredo-Cardenas et al., 1994). The anti-ENK used was a rabbit polyclonal antibody against leucine-enkephalin (ImmunoStar, Hudson, WI) whose specificity has also been shown previously (Reiner, 1987; Reiner et al., 2007).

EM immunolabeling for VGLUT1 or VGLUT2

Sections were pretreated with 1% sodium borohydride in 0.1 M PB for 30 minutes followed by incubation in 0.5% H_2O_2 solution in 0.1 M PB for 30 minutes. To carry out conventional single-label immunohistochemistry, sections were incubated overnight at room temperature in primary antiserum diluted 1:2000 (VGLUT1) or 1:2000 (VGLUT2) with 0.1M PB containing 10% normal horse serum, 4% normal goat serum, 1.5% bovine serum albumin, and 0.02% Triton X-100. Sections were then rinsed and incubated in biotinylated goat anti-guinea pig IgG diluted 1:100 (to detect guinea pig anti-VGLUT1 or VGLUT2) or biotinylated goat anti-rabbit IgG 1:100 (to detect rabbit anti-VGLUT2) in 0.1M PB (ph7.4) at room temperature for one hour, followed by incubation in the ABC complex in 0.1M PB (pH7.4) at room temperature for two hours. The sections were rinsed between secondary and ABC incubations in three five-minute washes of PB. Subsequent to the ABC incubation, the sections were rinsed with three to six 10-minute washes in 0.1M PB, and a peroxidase reaction using diaminobenzidine (DAB) carried out. After the PB rinses, the sections were immersed for 10 minutes in 0.05% DAB (Sigma, St. Louis, MO) in 0.1M PB (pH7.2). Hydrogen peroxide was then added to a final concentration of 0.01%, and the sections were incubated in this solution for an additional 10 minutes, and washed six times in PB. Some sections to be viewed by LM were mounted onto gelatin-coated slides, dried, and dehydrated, cleared with xylene, and coverslipped with Permount® (Fisher Scientific, Pittsburgh, PA). Tissue to be examined by EM was rinsed, dehydrated, and flat-embedded in plastic as described below.

Preparation of Tissue for EM

Following immunolabeling as described above, sections processed for EM viewing were rinsed in 0.1M sodium cacodylate buffer (pH 7.2), postfixed for 1 hour in 2% osmium tetroxide (OsO_4) in 0.1 M sodium cacodylate buffer, dehydrated in a graded series of ethyl alcohols, impregnated with 1% uranyl acetate in 100% alcohol, and flat-embedded in Spurr's resin (Electron Microscopy Sciences, Fort Washington, PA). For the flat-embedding, the sections were mounted on microslides pretreated with liquid releasing factor (Electron Microscopy Sciences, Fort Washington, PA). The Spurr's resin-embedded sections were examined light microscopically for the presence of VGLUT-immunolabeled axons and terminals in striatum. Pieces of embedded tissue were cut from the dorsolateral (motor) striatum and glued to carrier blocks, and ultrathin sections were cut from these specimens with a Reichert ultramicrotome. The sections were mounted on mesh grids, stained with 0.4% lead citrate and 4.0% uranyl acetate using an LKB Ultrastainer, and finally viewed and images captured with a JEOL 2000EX electron microscope.

VGLUT Antibodies Used

Both guinea pig VGLUT antisera are highly selective for their target antigens (Fremeau et al., 2001; Montana et al., 2004). The immunogen peptide used to produce the VGLUT1 antibody (Chemicon Cat. # AB5905) was rat VGLUT1 C-terminus, aa542–560. VGLUT1 antibody specificity has been demonstrated by Western blot analysis of rat cerebral cortex (Melone et al., 2005), and by immunogen block of retinal immunolabeling (Wässle et al., 2006). Melone et al. (2005) also showed that immunofluorescence with Chemicon anti-VGLUT1 nearly completely overlapped that for a previously well-characterized antibody against VGLUT1, although its target was called the brain-specific Na-dependent inorganic phosphate co-transporter (BNPI) at that time (Bellocchio et al., 1998). The immunogen peptide for the guinea pig VGLUT2 antibody (Chemicon Cat. # AB5907) was rat VGLUT2 C-terminus, AA 565–582, and Montana et al. (2004) showed specificity of the VGLUT2 antiserum in Western blots of rat cerebral cortex, and Wässle et al. (2006) reported that preadsorption of the VGLUT2 antiserum with its immunogen peptide blocked immunostaining in mouse retina. VGLUT2 is also known as the differentiation-associated Na-dependent inorganic phosphate co-transporter (DNPI). The immunogen for the rabbit VGLUT2 antibody (V2514, Sigma) was a synthetic peptide located near the C-terminus of rat VGLUT2 (amino acids 520–538). The sequence is identical in mouse and human VGLUT2 and has no homology to VGLUT1. Western blotting by the manufacturer confirms antibody specificity. A previous study of ours demonstrated that the immunolabeling in rat striatum for the two VGLUT2 antibodies used here show complete colocalization (Lei et al., 2013).

EM Analysis

Analysis and quantification was carried out on random fields using digital EM images. We focused on dorsolateral somatomotor striatum, which is poor in striosomes (although not entirely devoid) and the major target of intralaminar thalamus (Berendse and Groenewegen, 1990; Desban et al., 1993; Gerfen, 1992; Wang et al., 2007), and performed the analysis in the upper 5 microns of the sections, in which labeling was optimal. We avoided the very surface, where histology was poor. The size of terminals was determined by measuring them at their widest diameter parallel to and 0.1μm before the postsynaptic density, and spines were identifiable by their small size, continuity with dendrites, prominent postsynaptic density, and/or the presence of spine apparatus (Wilson et al., 1983). Dendrites were identifiable by their size, oval or elongate shape, and the presence of microtubules and mitochondria. For VGLUT1 and VGLUT2, counts of labeled and unlabeled synaptic terminals on spines and dendrites were made to ascertain the percent of axospinous and axodendritic terminals in mouse striatum that possess VGLUT1 or VGLUT2, and to

determine the abundance of each terminal type per unit area of striatum. The data are presented as group means (±SEM) for the various traits analyzed, unless otherwise stated. Analysis for each animal is based on 30–50 EM images per marker, which typically totaled >150 thalamic and cortical terminals per animal.

Volume Measurements

To evaluate the effect of the Q140 genotype on the volume of striatum, blinded image analysis was carried out (Reiner et al., 2007, 2012a). An image of each section in the one-in-six cresyl violet series of the LM hemisphere, mounted for each mouse at the time of sectioning, from the rostral telencephalic pole to just behind the anterior commissure, was captured using an Aperio ScanScope XT scanner. NIH ImageJ software was used to measure the area occupied by the striatum from the end of the olfactory bulb to the level just behind the anterior commissure. The striatum was defined by the contours of the external capsule and globus pallidus, while the boundaries of the lateral ventricles were readily evident. Section thickness and spacing were used to calculate volume from the area measurements.

Striatal Neuron Analysis

To assess injury to the striatal projection systems in the Q140 mice, blinded computer-assisted image analysis was carried out on immunolabeled striatal terminals in each of the three main striatal projection targets in rodents, the globus pallidus externus (GPe), the globus pallidus internus (GPi), and the substantia nigra (SN). For these studies, the extent and immunolabeling intensity of the striatally derived ENK fiber plexus in GPe and the striatally derived SP fiber plexuses in GPi and SN were analyzed using ImageJ software, as in our prior studies on human HD or HD animal models (Deng et al., 2004; Figueredo-Cardenas et al., 1994; Meade et al., 2000; Reiner et al., 2007, 2012a; Sun et al., 2002). Slides with sections immunolabeled for SP and ENK were scanned at 4800 dpi resolution (Epson Perfection 4490 Photo Scanner). Images of the entire GPe, GPi or SN were cropped bilaterally from the 1–2 (for GPi) or 4–6 (for GPe and SN) sections spanning their rostrocaudal extent in a one-in-twelve series. The immunolabeled fibers in GPe, GPi, or SN were highlighted, and their area and intensity (reflecting peptide abundance) determined using the automatic thresholding and optical density measuring capabilities of ImageJ software. Autothreshold uses the iterative isodata algorithm of Ridler and Calvard (1978) to set threshold at halfway between the foreground and background. To correct for slight variations in image intensity stemming from variations in lighting during scanning and/or from variations in the staining protocol, the background intensity of the captured images was standardized using the editing capabilities of ImageJ to a value of 100 on the 0–255 white-to-black gray scale employed by Image J. The region used to set the background intensity for each image was an area of unlabeled white matter within the field of view. For GPe and GPi, the external capsule was used, while for the substantia nigra the cerebral peduncle was used. Means per mouse were calculated for each structure and parameter from the individual measurements (Reiner et al., 2012a).

Statistics

Parametric t-tests were used to evaluate statistically significant differences between WT and Q140 mice within each of the three age groups examined for each of the parameters measured, all of which were independent. In the few instances in which terminals within a specific size range were compared between WT and Q140 mice by a t-test, a Bonferroni correction for multiple comparisons was applied. A Mann-Whitney U nonparametric t-test was performed for those few data sets that were not normally distributed.

Results

LM Studies - CLSM

We observed a significant decline in VGLUT1 and VGLUT2 terminals in striatum at the LM level at 12 months, but not earlier (Figs. 1, 2; Table 1). We evaluated three indicators of VGLUT fibers: 1) intensity of immunolabeling in the entire striatal field analyzed; 2) intensity of immunolabeling specifically in the labeled fibers; and 3) percent of the striatum covered by immunolabeled fibers. As can be seen, the overall intensity of striatal labeling for both VGLUT1 and VGLUT2 in the mutants was not significantly different than in the WT at either 1 month or 4 months. The overall striatal immunolabeling intensity measure reflects both fiber abundance and their VGLUT content. Using thresholding to examine selectively and separately the intensity and abundance of immunolabeled fibers, we also saw no significant difference for either VGLUT1 or VGLUT2 at the LM level between Q140 and WT at 1 month. Similar analysis for WT and Q140 at 4 months revealed a trend toward slight reductions in VGLUT1 and VGLUT2 terminal abundance in striatum (about 5–10%), but the reductions were not statistically significant. At 12 months, however, there was clear evidence that both VGLUT1 corticostriatal and VGLUT2 thalamostriatal terminals were reduced in abundance in Q140 HD mice. Overall VGLUT1 and VGLUT2 immunolabeling in striatum (VGLUT intensity for entire striatum) was significantly reduced by 15–20%, and the specific abundance of VGLUT2 thalamostriatal fibers and terminals was also significantly reduced by about 20%. Although the specific abundance of VGLUT1 corticostriatal fibers appears comparably reduced, this was not significant for this sample. The immunolabeling intensity for individual thresholded fibers showed a trend toward significant reduction ($p<0.055$) for both VGLUT1 and VGLUT2. Thus, the overall LM data indicate that both VGLUT1 and VGLUT2 are diminished at 12 months in Q140 heterozygotes, but they are not clearly diminished at 4 months.

EM Studies

Because of the inherent limitations of LM studies for specific assessment of synaptic terminal loss, we also performed quantitative EM studies. Four types of terminals were assessed at each of the three ages examined (1, 4, and 12 months): 1) VGLUT1 corticostriatal terminals on spines of striatal neurons; 2) VGLUT2 thalamostriatal terminals on spines of striatal neurons; 3) VGLUT1 corticostriatal terminals on dendrites of striatal neurons; and 4) VGLUT2 thalamostriatal terminals on dendrites of striatal neurons. Only terminals with an overt synaptic contact possessing a PSD (post-synaptic density) were measured, since all VGLUT terminals are excitatory and their synaptic contacts evidenced by the presence of vesicles in the terminal and a PSD in the spine or dendrite (Lei et al., 2013). Results for each terminal type are presented below in separate sections.

VGLUT1 Axospinous Terminals—VGLUT1 axospinous terminals showed an age-related increase in size and an age-related decrease in spatial frequency in WT mice, as shown in the mean size, mean spatial frequency, and size frequency distribution data (Figs. 3–6; Table 2). At 1 and 12 months, VGLUT1 axospinous terminals showed a bimodal size frequency distribution that may reflect a size difference between the small IT-type and large PT-type corticostriatal terminals (Reiner et al., 2010) (Fig. 5). No difference was seen between Q140 and WT mice at 1 or 4 months in mean size, mean spatial frequency, or size frequency distribution of VGLUT1 axospinous terminals (Fig. 5A–B; Table 2). At 12 months, however, a significant 27.3% reduction in the spatial abundance of VGLUT1 axospinous terminals was seen in the Q140 mice (Fig. 6). The size frequency distribution showed that the loss was in smaller terminals (0.4–0.5 μm), coinciding with the smaller of the two peaks seen in WT mice for VGLUT1 axospinous terminals (Fig. 5C). Note that the decline in spatial abundance of VGLUT1+ axospinous terminals in Q140 mice at 12 months

did not stem from a failure to label otherwise surviving corticostriatal terminals, but rather appears to reflect true terminal loss. VGLUT1-negative axospinous terminals were observed in the same frequency as VGLUT2+ axospinous terminals in WT and Q140 mice, meaning there was not a disproportionate increase in VGLUT1-unlabeled corticostriatal terminals in Q140 mice.

VGLUT2 Axospinous Terminals—As shown by their mean size and the peak of their size frequency distributions, VGLUT2 axospinous corticostriatal terminals became larger with age in WT mice, being larger at 4 months than 1 month (Figs. 7–9, Table 2). Associated with this growth in terminal size was also a decreased spatial frequency of the terminals. For example, axospinous VGLUT2 terminals are 10–20% less abundant per unit area at 4 months than 1 month. In general, a similar size increase is seen in the Q140 mice for VGLUT2 axospinous thalamostriatal terminals as in the WT mice. Note, however, there is a trend toward a 20% shortfall in the overall spatial abundance of VGLUT2 axospinous terminals in Q140 mice compared to WT at 1 month, and a significant 20% reduction in the overall spatial abundance of VGLUT2 axospinous terminals in Q140 mice at 4 months, and a comparable loss at 12 months (Fig. 6). This is shown in the table, in which abundance is expressed as synaptic terminals per square micron (Table 2). Comparisons for specific size ranges indicate that a loss occurs for smaller terminals in Q140 mice at all ages examined (Fig. 9). In the case of 1-month mice, the shortfall of VGLUT2 axospinous terminals occurs in the 0.3–0.6 μm range compared to WT mice (Fig. 9A), while the loss occurs in the 0.5–0.8 μm range at 4 and 12 months (Fig. 9B and 9C). The results thus indicate a shortfall in thalamostriatal axospinous terminals in Q140 striatum, beginning very early in the lifespan, already being evident at 1 month. Note that the shortfall in spatial abundance of VGLUT2+ axospinous terminals in Q140 mice did not stem from a failure to label otherwise surviving thalamostriatal terminals, but rather appears to reflect true terminal shortfall. VGLUT2-negative axospinous terminals were observed in the same frequency as VGLUT1+ axospinous terminals in WT and Q140 mice, meaning there was not a disproportionate increase in VGLUT2-unlabeled thalamostriatal terminals in Q140 mice.

VGLUT1 Axodendritic Terminals—VGLUT1 axodendritic terminals were the least common terminal type in WT mice, and showed a decline in abundance and increase in size from 1 month to 4 and 12 months. A similar trend was seen for VGLUT1 axodendritic terminals in Q140 mice, and no significant differences were seen between WT and Q140 at any age in spatial frequency or size (Table 2). Note, however, that due to the scarcity of this terminal type, results were somewhat variable.

VGLUT2 Axodendritic Terminals—VGLUT2 axodendritic terminal size showed a more complex pattern than VGLUT2 axospinous terminal size in WT mice (Figs. 10–11). VGLUT2 axodendritic terminals in WT mice were smaller in mean size at 1 month than at 4 and 12 months, and the spatial frequency data showed an overall decline of about 50% in their abundance from 1 to 4 months, which was maintained at 12 months (Fig. 6). The size frequency distribution data showed that the age-related decline in WT mice was in smaller (≤0.6 μm) VGLUT2 axodendritic terminals. Q140 mice showed a 40% shortfall in VGLUT2 axodendritic terminals at 1 month of age (Figs. 6 and 11A). The size frequency data shows the shortfall in Q140 mice to be in larger terminals. Since there was no significant increase in VGLUT2− negative axodendritic terminals at 1 month in Q140 mice, the shortfall in VGLUT2+ axodendritic terminals appears to represent a true deficiency in axodendritic thalamic input to striatum at this age. Unlike WT mice, Q140 mice showed no decline in the abundance of VGLUT2 axodendritic terminals from 1 to 4 months of age. As a result, no significant differences were evident between WT and Q140 mice in the spatial frequency of VGLUT2 axodendritic terminals at 4 and 12 months (Fig. 11B and 11C). Nonetheless, the

size frequency distributions of terminals showed that at 12 months, Q140 mice had more small (0.4μm) and fewer large (0.8μm) VGLUT2 axodendritic terminals than did WT mice. No such differences were seen at 4 months.

Comparisons among Terminal Types—The relative frequency of each terminal type as a percent of all four types summed together (axospinous VGLUT1, axodendritic VGLUT1, axospinous VGLUT2, and axodendritic VGLUT2) is shown in Table 3. These data highlight and detail the trends described above. At 1 month, a noteworthy relative deficiency in VGLUT2 axodendritic terminals is evident. Together with an under-representation of VGLUT2 axospinous terminals, this results in a relative over-preponderance of VGLUT1 axospinous terminals at 1 month. At 4 months, the 20% shortfall in VGLUT2 axospinous terminals yields a prominent under-representation of that terminal type compared to others and again a relative over-preponderance of VGLUT1 axospinous terminals. Finally, the larger loss of VGLUT1 axospinous than VGLUT2 axospinous terminals at 12 months in Q140 mice yields relative under-representation of VGLUT1 axospinous and relative over-representation of VGLUT2 axospinous terminals at that age. Additionally, a slight excess of VGLUT2 axodendritic terminals was evident in Q140 mice at 4 and 12 months.

LM Striatal Pathology Assessment

Striatal Volume—Note that precise estimates of the abundance of particular terminal types in striatum, and the impact of the Q140 mutation on this, need to take into account the reducing effects of age-related growth of striatal volume on VGLUT terminal spatial frequency, as well as the possible enhancing effects of disease-related striatal shrinkage on VGLUT terminal spatial frequency. To this end, we performed stereological volume measurements on the LM half of the brain for our cases. We found that the striatum in Q140 mice is not significantly different in its volume than it is in WT at any of three ages examined (Fig. 12). Thus, the area data for VGLUT terminal spatial frequency at each age accurately reflects the relative similarities or differences between WT and Q140 mice in VGLUT terminal abundance. The striatal volume for WT increased about 35% from 1 to 4 months as the mice grew to adulthood, and then another 10% by 12 months. Due to the increased volume, VGLUT1 axospinous and VGLUT2 axospinous terminals were about 20% more numerous in the entire striatum at 4 months and about 40% more numerous at 12 months than at 1 month, despite their lower spatial density at 4 and 12 months than at 1 month.

Striatal Projection Systems—Additionally, we measured the abundance of SP+ striatal terminals in GPi and substantia nigra, and ENK+ striatal terminals in GPe (Fig. 13). We found no differences between Q140 and WT in any of these measures, indicating that striatal projections neurons were not notably affected in the HD mutants at these ages. Thus, the loss of cortical and thalamic terminals that was observed at the ages studied did not obviously stem from striatal neuron loss at those ages, but rather was more likely to stem from input loss.

Discussion

Our EM results show early occurring deficiencies in the thalamic input to striatum and a later occurring loss of cortical input in the Q140 heterozygous mouse. The early occurring deficiency in thalamic input includes a 40% shortfall in thalamic input to dendrites at 1 month, and a 20% shortfall in thalamic input to spines that is also already manifest at 1 month and maintained at 4 and 12 months. By contrast, a 30% loss of cortical input is not evident until 12 months, and the loss is for axospinous terminals. Our LM data also show

overall reduction (i.e. not distinguishing axospinous and axodendritic terminals) in cortical input to striatum of about 20% at 12 months of age. Our LM and EM data for corticostriatal input loss are thus largely consistent with one another, indicating that corticostriatal neuron loss occurs between the ages of 4 and 12 months, and is significant (20–30%) by 12 months. Consistent with this time frame, slight cortical thinning (about 15%) is observed in heterozygous Q140 mice at 12 but not 9 months (Rising et al., 2011). Our EM data on thalamostriatal projections, however, detect a deficiency in VGLUT2+ input already at 1 month, but our LM data do not detect a VGLUT2+ input deficiency until 12 months. Our LM approach, however, could not distinguish between synaptic terminals and preterminal axons, while our EM approach only counted synaptic terminals. Thus, it may be that the arborization of VGLUT2+ thalamostriatal axons is largely normal in Q140 mice at 1 and 4 months, but these axons are deficient in the number of synaptic terminals they make. Our LM and EM data together suggest that the arborization of VGLUT2+ thalamostriatal axons and the number of terminals they form are both deficient by 12 months in Q140 mice. Taking cortical and thalamic input loss together, this yields an overall deficiency of about 25% in excitatory drive to striatum.

Our volumetric data indicate no significant differences between Q140 and WT in striatal volume over the 1–12 month age range, and our projection neuron immunolabeling indicate no significant differences between Q140 and WT in striatal projection neuron neurochemistry, suggesting no major loss in striatal projection neurons in the heterozygous Q140 mice studied here. Prior studies indicate no significant loss of striatal neurons in homozygous Q140 mice until >1 year of age (Hickey et al., 2008; Lerner et al., 2012), and a yet milder phenotype in heterozygous Q140 mice (Rising et al., 2011), further supporting the conclusion of no major striatal neuron loss in our Q140 mice over the age range studied here. Thus, it seems likely that the abnormalities in thalamic and cortical input to striatum in Q140 mice that we observed do not reflect loss of striatal neurons per se. Rather, it seems likely that loss or deficiency in the cortical or thalamic inputs to striatum per se accounts for our results. The loss of input could stem from impoverishment in axonal arborization and synapse formation by the cortical and thalamic inputs. Alternatively, loss of cortical or thalamic neurons may contribute to the deficient input to striatum in our Q140 mice. The latter, however, seems unlikely since cortical and thalamic neuron loss occurs after striatal neuron loss in HD, and we observed no evident striatal neuron loss in our Q140 mice. Our results thus indicate that an early occurring phenotype of heterozygous Q140 mice is a shortfall in the thalamic input to striatum, followed by later pruning of cortical input, in the likely absence of neuron loss from either cortex or thalamus, or their target the striatum. The early thalamic input shortfall raises the possibility that there is a developmental defect in striatal innervation by thalamus caused by the HD mutation in the Q140 mice. Consistent with this possibility, mild and non-progressive defects are evident in heterozygous Q140 mice in rearing and rotarod performance from a few months of age (Rising et al., 2011). These issues and their relevance to human HD are discussed in greater detail below.

Thalamic Input to Striatum in HD

Thalamic atrophy and hypometabolism have been reported in premanifest HD (Aylward et al., 2011; Feigin et al., 2007; Paulsen et al., 2004), although neuron loss has not been reported (Vonsattel et al., 1985). In symptomatic HD, both thalamic shrinkage and cell loss are evident (Byers et al., 1973; Douaud et al., 2006; Mann et al., 1993; Vonsattel, 2008; Vonsattel et al., 1985), with up to 50% interneuron loss in intralaminar thalamus late in disease (Heinsen et al., 1996, 1999), and atrophy of somatosensory thalamus as well (Dom et al., 1976). Imaging studies confirm that intralaminar thalamic nuclei projecting to frontal cortex and/or striatum undergo considerable atrophy in HD, and their atrophy is associated with cognitive (Kassubek et al., 2004a), and motor deficits (Ginestroni et al., 2010).

Consistent with the deficits associated with thalamostriatal projection system degeneration in HD, thalamic input to striatum is thought to play a role in attentional mechanisms concerning motor planning and preparedness (Smith et al., 2004). Various morphological and neurochemical thalamic abnormalities have also been observed in mouse models of HD, including increased GFAP expression, loss of the adhesion molecule tenascin-C, and loss of the synaptic protein complexin II in the parafascicular intralaminar nucleus of R6/2 transgenic mice (Freeman and Morton, 2004; Kusakabe et al., 2001). Of further note, striatal expression of the semaphorin 3E receptor Plexin-D1 is significantly reduced early in the lifespan of several transgenic or knock-in HD mice (Kuhn et al., 2007). This is of note because synapse formation between thalamostriatal terminals and direct pathway striatal projection neurons involves presynaptic semaphorin 3E – postsynaptic Plexin-D1 signaling (Ding et al., 2011), and the early underexpression of Plexin-D1 in HD mouse striatum may reflect a developmental defect and/or a loss in thalamostriatal connectivity for this neuron type. Significant abnormalities in striatal expression of Plexin-D1 are also seen early in the course of human HD as well (Strand et al., 2007). Similar HD-related impairment of developmental signaling could occur for thalamic input to indirect pathway neurons as well.

We observed an early occurring and seemingly sustained deficiency in thalamic input to striatal neuron dendrites in heterozygous Q140 mice. The shortfall was in the larger axodendritic thalamic terminals. That this shortfall was already evident at one month suggests that it may have been a developmental defect, since the thalamostriatal circuitry forms shortly after birth in rodents (Ding et al., 2011). The possibility of brain developmental defects has been suggested in human HD as well (Nopoulos et al., 2011). As thalamic input ends on the dendritic shafts of both cholinergic interneurons and striatal projection neurons (Bacci et al., 2002, 2004; Giorgi et al., 2001; Salin and Kachidian, 1998), we cannot know whether the missing thalamic axodendritic input in Q140 mice occurs for cholinergic interneurons or striatal projection neurons. A deficiency in thalamic input to spines as well was seen already at 1 month, and maintained at 4 months and 12 months. This too may represent a developmental defect, but possibly involve a progressive degenerative component as well. It is uncertain if the deficiency in thalamic input to Q140 striatum is a reflection of a reduced number of thalamic neurons, or a deficiency in their striatal branching. In any event, our results suggest that the thalamic shrinkage and hypometabolism observed in premanifest human HD may reflect early disease effects on thalamostriatal projection neurons, leading to deficient thalamostriatal connectivity that contributes to the concomitant striatal hypometabolism seen in human imaging studies. As noted above, the mild and non-progressive motor defects in heterozygous Q140 mice from a few months of age may in part stem from the early occurring thalamostriatal defect in these mice (Rising et al., 2011). This could also be the case for the behavioral abnormalities seen in homozygous Q140 mice in their first year of life before any demonstrated striatal pathology or neuron loss (Hickey et al., 2008; Lerner et al., 2012; Menalled et al., 2003).

Cortical Input to Striatum in HD

Numerous magnetic resonance imaging (MRI) and computed tomography (CT) imaging studies have noted regional cortical thinning and volume loss in premanifest HD, coupled with loss of cerebral white matter (Aylward et al., 2011; Ciarmiello et al., 2006; Dumas et al., 2012; Hobbs et al., 2010a; Kipps et al., 2005; Paulsen et al., 2006; Reading et al., 2005; Rosas et al., 2005, 2006). Additionally, cerebral white matter loss coincident with striatal hypometabolism (Ciarmiello et al., 2006; Grafton et al., 1992), and hypoactivation during task performance (Paulsen et al., 2004; Wolf et al., 2012) have been noted. Consistent with imaging studies of cerebrum, neuropathological investigation has reported loss of cerebral axons in premanifest HD (DiProspero et al., 2004). Although premanifest cortical neuron loss has not been quantified, it is generally thought to be minimal (Nopoulos, et al., 2010;

Vonsattel et al., 1985; Vonsattel and DiFiglia, 1998). Several authors have suggested that corticostriatal connectivity and drive becomes diminished in premanifest HD, increasingly so as onset nears (Wolf et al., 2008a,b, 2012). In this context then, our results in Q140 mice showing about 30% loss of corticostriatal terminals prior to striatal neuron loss and prominent motor decline suggest that corticostriatal synaptic pruning may occur during premanifest HD, and at least in part account for the observed abnormalities in striatal activity. Given the important role that cortical excitatory drive plays in the motor role of striatum, the early loss of corticostriatal input, together with a deficiency in thalamic input, may help explain the growing motor slowing evident in premanifest HD (Bechtel et al., 2010; Biglan et al., 2009; Blekher et al., 2004; de Boo et al., 1997; Delval et al., 2011; Kirkwood et al., 1999, 2000; Rao et al., 2008, 2011; Siemers et al., 1996; Tabrizi et al., 2011; Turner et al., 2011). Premanifest corticostriatal terminal loss might be expected as an early reflection of a pathogenic process that in symptomatic HD causes significant regional thinning of cerebral cortex (Douaud et al., 2006; Kassubek et al., 2004b; Muhlau et al., 2007; Rosas et al., 2003). The cortical shrinkage and white matter loss seen with imaging studies in symptomatic HD have been shown by neuropathological studies to reflect pyramidal projection neuron loss (Byers et al., 1973; Cudkowicz and Kowall, 1990; De La Monte et al., 1988; Passani et al., 1997; Selemon et al., 2004; Vonsattel et al., 1985). The neuron loss is progressive and can involve 50–70% of neurons in layers 3, 5, and 6 by late HD (Hedreen et al., 1991; MacDonald and Halliday, 2002; Sotrel et al., 1991). MRI and functional MRI studies show that cortical thinning in symptomatic HD involves both gray and whiter matter loss, is related to disease progress and to CAG repeat length (Jech et al., 2007; Kassubek et al., 2004b; Rosas et al., 2005; Squitieri et al., 2009), and is associated with loss of input to striatum (Bohanna et al., 2011; Kloppel et al., 2008; Wolf et al., 2008b). Unlike in our Q140 mice, however, striatal shrinkage is observed in premanifest HD individuals, increasingly so with proximity to clinically defined onset (Aylward et al., 1994, 1996, 2000; van den Bogaard et al., 2011; Henley et al., 2009; Hobbs et al., 2010b; Jurgens et al., 2008; Kipps et al., 2005; Paulsen et al., 2006; Wolf et al., 2012). It is uncertain if this is so because of a greater magnitude of striatal white matter loss in premanifest human HD, or because of some degree of early striatal neuron loss (Augood et al., 1997; Glass et al., 2000; Deng et al., 2004).

Although loss of corticostriatal input prior to significant striatal neuron loss has not been directly demonstrated neuropathologically in either human HD or in prior studies of mouse HD models, various neuropathological and physiological data from mouse models are consistent with our finding in premanifest Q140 mice. For example, loss of presynaptic markers such as Lin7b and synaptophysin from cortex, loss of postsynaptic markers such as PSD-95 from striatum, loss of dendritic spines from striatal projection neurons, and/or loss of excitatory synaptic terminals in striatum are observed in early symptomatic R6/2 and YAC128 mice (Cepeda et al., 2003; Cummings et al., 2010; Graham et al., 2009; Klapstein et al., 2001; Singaraja et al., 2011), consistent with loss of corticostriatal terminals by early symptomatic stages. The electrophysiological data from mouse models suggests that direct pathway neurons in particular are the striatal projection neuron type that shows reduced glutamatergic corticostriatal excitation (André et al., 2011a, b). Of interest with regard to our evidence for corticostriatal synaptic terminal loss prior to striatal projection neuron loss in Q140 mice, this striatal projection neuron type does not show loss in either R6/2 or YAC128 mice at the ages at which it shows electrophysiological signs of cortical disconnection (Benn et al., 2007; Reiner et al., 2012a,b).

The size of the corticostriatal terminals lost in Q140 mice suggests that it may, in fact, be the case for them as well that a substantial amount of the loss of corticostriatal terminals at 1 year occurs for direct pathway type striatal projection neurons. The corticostriatal input arises from two neuron types, an intratelencephalically projecting (IT) – type residing

predominantly in layer III and upper layer V, and a pyramidal tract (PT) - type located primarily in lower layer V (Cowan and Wilson, 1994; Levesque and Parent, 1998; Levesque et al., 1996a, b; Parent and Parent, 2006; Reiner et al., 2003; Wilson, 1987; Wright et al., 1999, 2001). We and other investigators have found in rats and monkeys that PT-type corticostriatal neurons preferentially contact striatal neurons projecting to the external segment of globus pallidus (GPe) with larger terminals, while IT-type cortical neurons preferentially target striatal neurons projecting to the internal pallidal segment (GPi) or the substantia nigra pars reticulata (SNr) with smaller terminals (Cepeda et al., 2008; Lei et al., 2004; Reiner et al., 2010). In the present study in 12-month old Q140 mice, the loss of corticostriatal terminals occurred selectively for smaller terminals, suggesting they might be IT-type terminals and preferentially lost from direct pathway type striatal neurons. If this is the case, this loss of drive to the “go” neurons of the direct pathway would be expected to cause behavioral hypoactivity, which is observed as a major symptom as Q140 mice age (Hickey et al., 2008; Menalled et al., 2003; Rising et al., 2011). If a similar event occurs in humans, it could help explain the slowing of movement initiation and execution seen in premanifest HD.

In both R6/2 and YAC128 HD mice, however, the eventual loss in corticostriatal drive to the striatum is preceded by very early corticostriatal hyperactivity (André et al., 2011a; Cepeda et al., 2003; Joshi et al., 2009). Although it is uncertain if the early enhanced corticostriatal synaptic activity reflects enhanced cortical neuron activity or enhanced glutamate release due to corticostriatal terminal dysfunction, the large amplitude synaptic events together with the higher membrane input resistance and depolarized resting membrane potentials of striatal projection neurons is consistent with the increased activation of striatal projection neurons early in progression in HD mice (Rebec et al., 2006). The electrophysiological data from mouse models suggests that direct pathway neurons in particular are the striatal projection neuron type that shows early enhanced and later reduced glutamatergic corticostriatal excitation (André et al., 2011a, b). By contrast, indirect pathway striatal projection neurons show neither the early cortically driven hyperexcitability nor the late hypoexcitability. Despite any loss of excitatory input, striatal projection neurons in HD mice remain hyperexcitable, since they are more depolarized at rest, and have elevated input resistances (Cepeda et al., 2003; Estrada-Sanchez and Rebec, 2013; Singaraja et al., 2011). Thus, loss of cortical input may, in part, be a regulated event that prevents striatal projection neuron overexcitation, rather than strictly a reflection of cortical neuron pathology. The possibility that cortical input loss is preferential for direct pathway striatal projection neurons is of interest in light of the possibility that the cortical input loss is neuroprotective. Direct pathway projection neurons projecting to GPi are the most resistant projection neuron type in HD (Deng et al., 2004), and a downregulation in excitatory cortical input to them may explain not only why direct pathway striato-GPi neurons resist death better in human HD, but also may explain the emergence of resistance to corticostriatal excitotoxicity as HD mice age (Graham et al., 2009; Hansson et al., 1999, 2001).

Acknowledgments

We thank Marion Joni, Kathy Troughton, and Yunming Hu for technical assistance. Supported by the CHDIF (AR), NIH NS57722, and The Methodist Hospitals Endowed Professorship in Neuroscience (AR).

References

Albin RL, Qin Y, Young AB, Penney JB, Chesselet MF. Preproenkephalin messenger RNA-containing neurons in striatum of patients with symptomatic and presymptomatic Huntington's disease: an in situ hybridization study. Ann. Neurol. 1991; 30:542–549. [PubMed: 1838677]

Albin RL, Young AB, Penney JB. The functional anatomy of basal ganglia disorders. Trends Neurosci. 1989; 12:366–375. [PubMed: 2479133]

André VM, Cepeda C, Fisher YE, Huynh M, Bardakjian N, Singh S, Yang XW, Levine MS. Differential electrophysiological changes in striatal output neurons in Huntington's disease. J. Neurosci. 2011a; 31:1170–1182. [PubMed: 21273402]

André VM, Fisher YE, Levine MS. Altered Balance of Activity in the Striatal Direct and Indirect Pathways in Mouse Models of Huntington's Disease. Front. Syst. Neurosci. 2011b; 5:46. [PubMed: 21720523]

Augood SJ, Faull RL, Emson PC. Dopamine D1 and D2 receptor gene expression in the striatum in Huntington's disease. Ann. Neurol. 1997; 42:215–221. [PubMed: 9266732]

Aylward EH, Brandt J, Codori AM, Mangus RS, Barta PE, Harris GJ. Reduced basal ganglia volume associated with the gene for Huntington's disease in asymptomatic at-risk persons. Neurology. 1994; 44:823–828. [PubMed: 8190282]

Aylward EH, Codori AM, Barta PE, Pearlson GD, Harris GJ, Brandt J. Basal ganglia volume and proximity to onset in presymptomatic Huntington disease. Arch. Neurol. 1996; 53:1293–1296. [PubMed: 8970459]

Aylward EH, Codori AM, Rosenblatt A, Sherr M, Brandt J, Stine OC, Barta PE, Pearlson GD, Ross CA. Rate of caudate atrophy in presymptomatic and symptomatic stages of Huntington's disease. Mov. Disord. 2000; 15:552–560. [PubMed: 10830423]

Aylward EH, Nopoulos PC, Ross CA, Langbehn DR, Pierson RK, Mills JA, Johnson HJ, Magnotta VA, Juhl AR, Paulsen JS. PREDICT-HD Investigators and Coordinators of Huntington Study Group. Longitudinal change in regional brain volumes in prodromal Huntington disease. J. Neurol. Neurosurg. Psychiatry. 2011; 82:405–410. [PubMed: 20884680]

Bacci JJ, Kerkerian-Le Goff L, Salin P. Effects of intralaminar thalamic nuclei lesion on glutamic acid decarboxylase (GAD65 and GAD67) and cytochrome oxidase subunit I mRNA expression in the basal ganglia of the rat. Eur. J. Neurosci. 2002; 15:1918–1928. [PubMed: 12099898]

Bacci JJ, Kachidian P, Kerkerian-Le Goff L, Salin P. Intralaminar thalamic nuclei lesions: widespread impact on dopamine denervation-mediated cellular defects in the rat basal ganglia. J. Neuropathol. Exp. Neurol. 2004; 63:20–31. [PubMed: 14748558]

Bechtel N, Scahill RI, Rosas HD, Acharya T, van den Bogaard SJ, Jauffret C, Say MJ, Sturrock A, Johnson H, Onorato CE, Salat DH, Durr A, Leavitt BR, Roos RA, Landwehrmeyer GB, Langbehn DR, Stout JC, Tabrizi SJ, Reilmann R. Tapping linked to function and structure in premanifest and symptomatic Huntington disease. Neurology. 2010; 75:2150–2160. [PubMed: 21068430]

Bellocchio EE, Hu H, Pohorille A, Chan J, Pickel VM, Edwards RH. The localization of the brain-specific inorganic phosphate transporter suggests a specific presynaptic role in glutamatergic transmission. J. Neurosci. 1998; 18:8648–8659. [PubMed: 9786972]

Benn CL, Slow EJ, Farrell LA, Graham R, Deng Y, Hayden MR, Cha JHJ. Glutamate receptor abnormalities in the YAC128 transgenic mouse model of Huntington’s disease. Neuroscience. 2007; 147:354–372. [PubMed: 17544587]

Berendse HW, Groenewegen HJ. Organization of the thalamostriatal projections in the rat, with special emphasis on the ventral striatum. J. Comp. Neurol. 1990; 299:187–228. [PubMed: 2172326]

Biglan KM, Ross CA, Langbehn DR, Aylward EH, Stout JC, Queller S, Carlozzi NE, Duff K, Beglinger LJ, Paulsen JS. PREDICT-HD Investigators of the Huntington Study Group. Motor abnormalities in premanifest persons with Huntington's disease: the PREDICT-HD study. Mov. Disord. 2009; 24:1763–1772. [PubMed: 19562761]

Blekher TM, Yee RD, Kirkwood SC, Hake AM, Stout JC, Weaver MR, Foroud TM. Oculomotor control in asymptomatic and recently diagnosed individuals with the genetic marker for Huntington's disease. Vision Res. 2004; 44:2729–2736. [PubMed: 15358067]

Bohanna I, Georgiou-Karistianis N, Egan GF. Connectivity-based segmentation of the striatum in Huntington’s disease: Vulnerability of motor pathways. Neurobio. Dis. 2011; 42:475–481.

Byers RK, Gilles FH, Fung C. Huntington's disease in children. Neuropathologic study of four cases. Neurology. 1973; 23:561–569. [PubMed: 4267989]

Cepeda C, André VM, Yamazaki I, Wu N, Kleiman-Weiner M, Levine MS. Differential electrophysiological properties of dopamine D1 and D2 receptor-containing striatal medium-sized spiny neurons. Eur. J. Neurosci. 2008; 27:671–682. [PubMed: 18279319]

Cepeda C, Hurst RS, Calvert CR, Hernández-Echeagaray E, Nguyen OK, Jocoy E, Christian LJ, Ariano MA, Levine MS. Transient and progressive electrophysiological alterations in the corticostriatal pathway in a mouse model of Huntington's disease. J. Neurosci. 2003; 23:961–969. [PubMed: 12574425]

Ciarmiello A, Cannella M, Lastoria S, Simonelli M, Frati L, Rubinsztein DC, Squitieri F. Brain white-matter volume loss and glucose hypometabolism precede the clinical symptoms of Huntington's disease. J. Nucl. Med. 2006; 47:215–222. [PubMed: 16455626]

Cowan RL, Wilson CJ. Spontaneous firing patterns and axonal projections of single corticostriatal neurons in the rat medial agranular cortex. J. Neurophysiol. 1994; 71:17–32. [PubMed: 8158226]

Cudkowicz M, Kowall NW. Degeneration of pyramidal projection neurons in Huntington's disease cortex. Ann. Neurol. 1990; 27:200–204. [PubMed: 2138444]

Cummings DM, Cepeda C, Levine MS. Alterations in striatal synaptic transmission are consistent across genetic mouse models of Huntington's disease. ASN Neuro. 2010; 2:e00036. [PubMed: 20585470]

de Boo GM, Tibben A, Lanser JB, Jennekens-Schinkel A, Hermans J, Maat-Kievit A, Roos RA. Early cognitive and motor symptoms in identified carriers of the gene for Huntington disease. Arch. Neurol. 1997; 54:1353–1357. [PubMed: 9362982]

De La Monte SM, Vonsattel JP, Richardson EP Jr. Morphometric demonstration of atrophic changes in the cerebral cortex, white matter, and neostriatum in Huntington's disease. J. Neuropathol. Exp. Neurol. 1988; 47:516–525. [PubMed: 2971785]

Delval A, Bleuse S, Simonin C, Delliaux M, Rolland B, Destee A, Defebvre L, Krystkowiak P, Dujardin K. Are gait initiation parameters early markers of Huntington's disease in pre-manifest mutation carriers? Gait & Posture. 2011; 34:202–207. [PubMed: 21616667]

Deng YP, Albin RL, Penney JB, Young AB, Anderson KD, Reiner A. Differential loss of striatal projection systems in Huntington's disease: a quantitative immunohistochemical study. J. Chem. Neuroanat. 2004; 27:143–164. [PubMed: 15183201]

Deng YP, Lei WL, Reiner A. Differential localization in rats of D1 and D2 dopamine receptors on striatal projection neuron types identified by retrograde labeling. J. Chem. Neuroanat. 2006; 32:101–116. [PubMed: 16914290]

Deng YP, Xie JP, Wang HB, Lei WL, Chen Q, Reiner A. Differential localization of the GluR1 and GluR2 subunits of the AMPA-type glutamate receptor among striatal neuron types in rats. J. Chem. Neuroanat. 2007; 33:167–192. [PubMed: 17446041]

Desban M, Kemel ML, Glowinski J, Gauchy C. Spatial organization of patch and matrix compartments in the rat striatum. Neuroscience. 1993; 57:661–667. [PubMed: 8309529]

Ding JB, Oh WJ, Sabatini BL, Gu C. Semaphorin 3E-Plexin-D1 signaling controls pathway-specific synapse formation in the striatum. Nat. Neurosci. 2011; 15:215–223. [PubMed: 22179111]

DiProspero NA, Chen EY, Charles V, Plomann M, Kordower JH, Tagle DA. Early changes in Huntington's disease patient brains involve alterations in cytoskeletal and synaptic elements. J. Neurocytol. 2004; 33:517–533. [PubMed: 15906159]

Dom R, Malfroid M, Baro F. Neuropathology of Huntington's chorea. Studies of the ventrobasal complex of the thalamus. Neurology. 1976; 26:64–68. [PubMed: 128708]

Douaud G, Gaura V, Ribeiro MJ, Lethimonnier F, Maroy R, Verny C, Krystkowiak P, Damier P, Bachoud-Levi AC, Hantraye P, Remy P. Distribution of grey matter atrophy in Huntington's disease patients: a combined ROI-based and voxel-based morphometric study. Neuroimage. 2006; 32:1562–1575. [PubMed: 16875847]

Dumas EM, van den Bogaard SJ, Ruber ME, Reilman RR, Stout JC, Craufurd D, Hicks SL, Kennard C, Tabrizi SJ, van Buchem MA, van der Grond J, Roos RA. Early changes in white matter pathways of the sensorimotor cortex in premanifest Huntington's disease. Hum. Brain Mapp. 2012; 33:203–212. [PubMed: 21264990]

Estrada-Sanchez A, Rebec VG. Role of cerebral cortex in the neuropathology of Huntington’s disease. Front. Neural Circuits. 2013; 7:19. [PubMed: 23423362]

Feigin A, Tang C, Ma Y, Mattis P, Zgaljardic D, Guttman M, Paulsen JS, Dhawan V, Eidelberg D. Thalamic metabolism and symptom onset in preclinical Huntington's disease. Brain. 2007; 130:2858–2867. [PubMed: 17893097]

Figueredo-Cardenas G, Anderson KD, Chen Q, Veeman CL, Reiner A. Relative survival of striatal projection neurons and interneurons after intrastriatal injection of quinolinic acid in rats. Exp. Neurol. 1994; 129:37–56. [PubMed: 7925841]

Freeman W, Morton AJ. Regional and progressive changes in brain expression of complexin II in a mouse transgenic for the Huntington's disease mutation. Brain Res, Bull. 2004; 63:45–55. [PubMed: 15121238]

Fremeau RT, Troyer MD, Pahner I, Nygaard GO, Tran CH, Reiner RJ, Bellocchio EE, Fortin D, Storm-Mathisen J, Edwards RH. The expression of vesicular glutamate transporters defines two classes of excitatory synapse. Neuron. 2001; 31:247–260. [PubMed: 11502256]

Fremeau RT, Voglmaier S, Seal RP, Edwards RH. VGLUTs define subsets of excitatory neurons and suggest novel roles for glutamate. Trends Neurosci. 2004; 27:98–103. [PubMed: 15102489]

Fujiyama F, Kuramoto E, Okamoto K, Hioki H, Furuta T, Zhou L, Nomura S, Kaneko T. Presynaptic localization of an AMPA-type glutamate receptor in corticostriatal and thalamostriatal axon terminals. Eur. J. Neurosci. 2004; 20:3322–3330. [PubMed: 15610164]

Gerfen CR. The neostriatal mosaic: multiple levels of compartmental organization in the basal ganglia. Ann. Rev. Neurosci. 1992; 15:285–320. [PubMed: 1575444]

Ginestroni A, Battaglini M, Diciotti S, Della Nave R, Mazzoni LN, Tessa C, Giannelli M, Piacentini S, De Stefano N, Mascalchi M. Magnetization Transfer MR Imaging Demonstrates Degeneration of the Subcortical and Cortical Gray Matter in Huntington Disease. Am. J. Neuroradiol. 2010; 31:1807–1812. [PubMed: 20813872]

Giorgi S, Rimoldi M, Consolo S. Parafascicular thalamic nucleus deafferentation reduces c-fos expression induced by dopamine D-1 receptor stimulation in rat striatum. Neuroscience. 2001; 103:653–661. [PubMed: 11274785]

Glass M, Dragunow M, Faull RLM. The pattern of neurodegeneration in Huntington’s disease: a comparative study of cannabinoid, dopamine, adenosine and GABAa receptor alterations in the human basal ganglia in Huntington’s disease. Neuroscience. 2000; 97:505–519. [PubMed: 10828533]

Grafton ST, Mazziotta JC, Pahl JJ, St George-Hyslop P, Haines JL, Gusella J, Hoffman JM, Baxter LR, Phelps ME. Serial changes of cerebral glucose metabolism and caudate size in persons at risk for Huntington's disease. Arch. Neurol. 1992; 49:1161–1167. [PubMed: 1444883]

Graham RK, Pouladi MA, Joshi P, Lu G, Deng Y, Wu NP, Figueroa BE, Metzler M, André VM, Slow EJ, Raymond L, Friedlander R, Levine MS, Leavitt BR, Hayden MR. Differential susceptibility to excitotoxic stress in YAC128 mouse models of Huntington disease between initiation and progression of disease. J. Neurosci. 2009; 29:2193–2204. [PubMed: 19228972]

Groenewegen HJ, Berendse HW. The specificity of the ‘nonspecific’ midline and intralaminar thalamic nuclei. Trends Neurosci. 1994; 17:52–57. [PubMed: 7512768]

Hansson O, Guatteo E, Mercuri NB, Bernardi G, Li XJ, Castilho RF, Brundin P. Resistance to NMDA toxicity correlates with appearance of nuclear inclusions, behavioural deficits and changes in calcium homeostasis in mice transgenic for exon 1 of the huntington gene. Eur. J. Neurosci. 2001; 14:1492–1504. [PubMed: 11722611]

Hansson O, Petersén A, Leist M, Nicotera P, Castilho RF, Brundin P. Transgenic mice expressing a Huntington's disease mutation are resistant to quinolinic acid-induced striatal excitotoxicity. Proc. Natl. Acad. Sci. U. S. A. 1999; 96:8727–8732. [PubMed: 10411943]

Hedreen JC, Peyser CE, Folstein SE, Ross CA. Neuronal loss in layers V and VI of cerebral cortex in Huntington's disease. Neurosci. Lett. 1991; 133:257–261. [PubMed: 1840078]

Heinsen H, Rüb U, Bauer M, Ulmar G, Bethke B, Schüler M, Böcker F, Eisenmenger W, Götz M, Korr H, Schmitz C. Nerve cell loss in the thalamic mediodorsal nucleus in Huntington's disease. Acta Neuropathol. 1999; 97:613–622. [PubMed: 10378380]

Heinsen H, Rüb U, Gangnus D, Jungkunz G, Bauer M, Ulmar G, Bethke B, Schüler M, Böcker F, Eisenmenger W, Götz M, Strik M. Nerve cell loss in the thalamic centromedian-parafascicular complex in patients with Huntington's disease. Acta Neuropathol. 1996; 91:161–168. [PubMed: 8787149]

Henley SM, Wild EJ, Hobbs NZ, Scahill RI, Ridgway GR, Macmanus DG, Barker RA, Fox NC, Tabrizi SJ. Relationship between CAG repeat length and brain volume in premanifest and early Huntington's disease. J. Neurol. 2009; 256:203–212. [PubMed: 19266143]

Herzog E, Bellenchi GC, Gras C, Bernard V, Ravassard P, Bedet C, Gasnier B, Giros B, El Mestikawy S. The existence of a second vesicular glutamate transporter specifies subpopulations of glutamatergic neurons. J. Neurosci. 2001; 21(RC81):1–6.

Hickey MA, Kosmalska A, Enayati J, Cohen R, Zeitlin S, Levine MS, Chesselet MF. Extensive early motor and non-motor behavioral deficits are followed by striatal neuronal loss in knock-in Huntington's disease mice. Neuroscience. 2008; 157:280–295. [PubMed: 18805465]

Hobbs NZ, Barnes J, Frost C, Henley SM, Wild EJ, Macdonald K, Barker RA, Scahill RI, Fox NC, Tabrizi SJ. Onset and progression of pathologic atrophy in Huntington disease: a longitudinal MR imaging study. AJNR Am. J. Neuroradiol. 2010a; 31:1036–1041. [PubMed: 20150305]

Hobbs NZ, Henley SM, Ridgway GR, Wild EJ, Barker RA, Scahill RI, Barnes J, Fox NC, Tabrizi SJ. The progression of regional atrophy in premanifest and early Huntington's disease: a longitudinal voxel-based morphometry study. J. Neurol. Neurosurg. Psychiatry. 2010b; 81:756–763. [PubMed: 19955112]

Jech R, Klempír J, Vymazal J, Zidovská J, Klempírová O, Růzicka E, Roth J. Variation of selective gray and white matter atrophy in Huntington's disease. Mov. Disord. 2007; 22:1783–1789. [PubMed: 17579363]

Joshi PR, Wu NP, André VM, Cummings DM, Cepeda C, Joyce JA, Carroll JB, Leavitt BR, Hayden MR, Levine MS, Bamford NS. Age-dependent alterations of corticostriatal activity in the YAC128 mouse model of Huntington disease. J. Neurosci. 2009; 29:2414–2427. [PubMed: 19244517]

Jurgens CK, van de Wiel L, van Es AC, Grimbergen YM, Witjes-Ané MN, van der Grond J, Middelkoop HA, Roos RA. Basal ganglia volume and clinical correlates in 'preclinical' Huntington's disease. J. Neurol. 2008; 255:1785–1791. [PubMed: 19156490]

Kassubek J, Bernhard Landwehrmeyer G, Ecker D, Juengling FD, Muche R, Schuller S, Weindl A, Peinemann A. Global cerebral atrophy in early stages of Huntington's disease: quantitative MRI study. Neuroreport. 2004a; 15:363–365. [PubMed: 15076769]

Kassubek J, Juengling FD, Kioschies T, Henkel K, Karitzky J, Kramer B, Ecker D, Andrich J, Saft C, Kraus P, Aschoff AJ, Ludolph AC, Landwehrmeyer GB. Topography of cerebral atrophy in early Huntington's disease: a voxel based morphometric MRI study. J. Neurol. Neurosurg. Psychiatry. 2004b; 75:213–220. [PubMed: 14742591]

Kato S, Kuramochi M, Kobayashi K, Fukabori R, Okada K, Uchigashima M, Watanabe M, Tsutsui Y, Kobayashi K. Selective neural pathway targeting reveals key roles of thalamostriatal projection in the control of visual discrimination. J. Neurosci. 2011; 31:17169–17179. [PubMed: 22114284]

Kipps CM, Duggins AJ, Mahant N, Gomes L, Ashburner J, McCusker EA. Progression of structural neuropathology in preclinical Huntington's disease: a tensor based morphometry study. J. Neurol. Neurosurg. Psychiatry. 2005; 76:650–655. [PubMed: 15834021]

Kirkwood SC, Siemers E, Stout JC, Hodes ME, Conneally PM, Christian JC, Foroud T. Longitudinal cognitive and motor changes among presymptomatic Huntington disease gene carriers. Arch. Neurol. 1999; 56:563–568. [PubMed: 10328251]

Kirkwood SC, Siemers E, Bond C, Conneally PM, Christian JC, Foroud T. Confirmation of subtle motor changes among presymptomatic carriers of the Huntington disease gene. Arch. Neurol. 2000; 57:1040–1044. [PubMed: 10891987]

Klapstein GJ, Fisher RS, Zanjani H, Cepeda C, Jokel ES, Chesselet MF, Levine MS. Electrophysiological and morphological changes in striatal spiny neurons in R6/2 Huntington's disease transgenic mice. J. Neurophysiol. 2001; 86:2667–2677. [PubMed: 11731527]

Klöppel S, Draganski B, Golding CV, Chu C, Nagy Z, Cook PA, Hicks SL, Kennard C, Alexander DC, Parker GJ, Tabrizi SJ, Frackowiak RS. White matter connections reflect changes in voluntary-guided saccades in pre-symptomatic Huntington's disease. Brain. 2008; 131:196–204. [PubMed: 18056161]

Kuhn A, Goldstein DR, Hodges A, Strand AD, Sengstag T, Kooperberg C5, Becanovic K, Pouladi MA, Sathasivam K, Cha JHJ, Hannan AJ, Hayden MR, Leavitt BR, Dunnett SB, Ferrante RJ, Albin R, Shelbourne P, Delorenzi M, Augood SJ, Faull RLM, Olson JM, Bates GP, Jones L,

Luthi-Carter R. Mutant huntingtin's effects on striatal gene expression in mice recapitulate changes observed in human Huntington's disease brain and do not differ with mutant huntingtin length or wild-type huntingtin dosage. Hum. Mol. Gen. 2007; 16:1845–1861. [PubMed: 17519223]

Kusakabe M, Mangiarini L, Laywell ED, Bates GP, Yoshiki A, Hiraiwa N, Inoue J, Steindler DA. Loss of cortical and thalamic neuronal tenascin-C expression in a transgenic mouse expressing exon 1 of the human Huntington disease gene. J. Comp. Neurol. 2001; 430:485–500. [PubMed: 11169482]

Lei W, Deng YP, Liu BB, Mu SH, Guley NM, Wong T, Reiner A. A confocal laser scanning microscopy and ultrastructural study of VGLUT2 thalamic input to striatal projection neurons in rats. J. Comp. Neurol. 2013; 521:1354–1377. [PubMed: 23047588]

Lei W, Jiao Y, Del Mar N, Reiner A. Evidence for differential cortical input to direct pathway versus indirect pathway striatal projection neurons in rats. J. Neurosci. 2004; 24:8289–8299. [PubMed: 15385612]

Lerner RP, Trejo Martinez L, del C, Zhu C, Chesselet MF, Hickey MA. Striatal atrophy and dendritic alterations in a knock-in mouse model of Huntington's disease. Brain Res Bull. 2012; 87:571–578. [PubMed: 22326483]

Levesque M, Charara A, Gagnon S, Parent A, Deschenes M. Corticostriatal projections from layer V cells in rat are collaterals of long-range corticofugal axons. Brain Res. 1996a; 709:311–315. [PubMed: 8833768]

Lévesque M, Gagnon S, Parent A, Deschênes M. axonal arborizations of corticostriatal and corticothalamic fibers arising from the second somatosensory area in the rat. Cereb. Cortex. 1996b; 6:759–770. [PubMed: 8922332]

Lévesque M, Parent A. Axonal arborization of corticostriatal and corticothalamic fibers arising from prelimbic cortex in the rat. Cereb Cortex. 1998; 8:602–813. [PubMed: 9823481]

Macdonald V, Halliday G. Pyramidal cell loss in motor cortices in Huntington's disease. Neurobiol. Dis. 2002; 10:378–386. [PubMed: 12270698]

Mann DM, Oliver R, Snowden JS. The topographic distribution of brain atrophy in Huntington's disease and progressive supranuclear palsy. Acta Neuropathol. 1993; 85:553–559. [PubMed: 8493863]

Meade CA, Figueredo-Cardenas G, Fusco F, Nowak TS Jr, Pulsinelli WA, Reiner A. Transient global ischemia in rats yields striatal projection neuron and interneuron loss resembling that in Huntington's disease. Exp. Neurol. 2000; 166:307–323. [PubMed: 11085896]

Melone M, Burette A, Weinberg RJ. Light microscopic identification and immunocytochemical characterization of glutamatergic synapses in brain sections. J. Comp. Neurol. 2005; 492:495–509. [PubMed: 16228991]

Menalled LB, Sison JD, Dragatsis I, Zeitlin S, Chesselet MF. Time course of early motor and neuropathological anomalies in a knock-in mouse model of Huntington's disease with 140 CAG repeats. J. Comp. Neurol. 2003; 465:11–26. [PubMed: 12926013]

Montana N, Ni Y, Sunjara V, Hua X, Parpura V. Vesicular glutamate transporter-dependent glutamate release from astrocytes. J. Neurosci. 2004; 24:2633–2642. [PubMed: 15028755]

Mühlau M, Weindl A, Wohlschläger AM, Gaser C, Städtler M, Valet M, Zimmer C, Kassubek J, Peinemann A. Voxel-based morphometry indicates relative preservation of the limbic prefrontal cortex in early Huntington disease. J. Neural. Transm. 2007; 114:367–372. [PubMed: 17024326]

Nopoulos PC, Aylward EH, Ross CA, Johnson HJ, Magnotta VA, Juhl AR, Pierson RK, Mills J, Langbehn DR, Paulsen JS. PREDICT-HD Investigators Coordinators of Huntington Study Group (HSG). Cerebral cortex structure in prodromal Huntington disease. Neurobiol. Dis. 2010; 40:544–554. [PubMed: 20688164]

Nopoulos PC, Aylward EH, Ross CA, Mills JA, Langbehn DR, Johnson HJ, Magnotta VA, Pierson RK, Beglinger LJ, Nance MA, Barker RA, Paulsen JS. PREDICT-HD Investigators and Coordinators of the Huntington Study Group. Smaller intracranial volume in prodromal Huntington's disease: evidence for abnormal neurodevelopment. Brain. 2011; 134:137–142. [PubMed: 20923788]

Parent M, Parent A. Single-axon tracing study of corticostriatal projections arising from primary motor cortex in primates. J. Comp. Neurol. 2006; 496:202–213. [PubMed: 16538675]

Passani LA, Vonsattel JP, Carter RE, Coyle JT. N-acetylaspartylglutamate, N-acetylaspartate, and N-acetylated alpha-linked acidic dipeptidase in human brain and their alterations in Huntington and Alzheimer's diseases. Mol. Chem. Neuropathol. 1997; 31:97–118. [PubMed: 9376025]

Paulsen JS, Magnotta VA, Mikos AE, Paulson HL, Penziner E, Andreasen NC, Nopoulos PC. Brain structure in preclinical Huntington's disease. Biol. Psychiatry. 2006; 59:57–63. [PubMed: 16112655]

Paulsen JS, Zimbelman JL, Hinton SC, Langbehn DR, Leveroni CL, Benjamin ML, Reynolds NC, Rao SM. fMRI biomarker of early neuronal dysfunction in presymptomatic Huntington's Disease. AJNR Am. J. Neuroradiol. 2004; 25:1715–1721. [PubMed: 15569736]

Rao AK, Muratori L, Louis ED, Moskowitz CB, Marder KS. Spectrum of gait impairments in presymptomatic and symptomatic Huntington's disease. Mov. Disord. 2008; 23:1100–1107. [PubMed: 18412252]

Rao AK, Gordon AM, Marder KS. Coordination of fingertip forces during precision grip in premanifest Huntington's disease. Mov. Disord. 2011; 26:862–869. [PubMed: 21394785]

Reading SA, Yassa MA, Bakker A, Dziorny AC, Gourley LM, Yallapragada V, Rosenblatt A, Margolis RL, Aylward EH, Brandt J, Mori S, van Zijl P, Bassett SS, Ross CA. Regional white matter change in pre-symptomatic Huntington's disease: a diffusion tensor imaging study. Psychiatry Res. 2005; 140:55–62. [PubMed: 16199141]

Rebec GV, Conroy SK, Barton SJ. Hyperactive striatal neurons in symptomatic Huntington R6/2 mice: variations with behavioral state and repeated ascorbate treatment. Neuroscience. 2006; 137:327–336. [PubMed: 16257492]

Reiner A. The distribution of proenkephalin-derived peptides in the central nervous system of turtle. J. Comp. Neurol. 1987; 259:65–91. [PubMed: 3294930]

Reiner A, Albin RL, Anderson KD, D'Amato CJ, Penney JB, Young AB. Differential loss of striatal projection neurons in Huntington disease. Proc. Natl. Acad. Sci. U S A. 1988; 85:5733–5737. [PubMed: 2456581]

Reiner A, Anderson KD. The patterns of neurotransmitter and neuropeptide co-occurrence among striatal projection neurons: conclusions based on recent findings. Brain Res. Rev. 1990; 15:251–265. [PubMed: 1981156]

Reiner A, Del Mar N, Deng YP, Meade CA, Sun Z, Goldowitz D. R6/2 Neurons with intranuclear inclusions survive for prolonged periods in the brains of chimeric mice. J. Comp. Neurol. 2007; 505:603–737. [PubMed: 17948889]

Reiner A, Hart NM, Lei W, Deng Y. Corticostriatal projection neurons - dichotomous types and dichotomous functions. Front. Neuroanat. 2010; 4:142. [PubMed: 21088706]

Reiner A, Jiao Y, Del Mar N, Laverghetta AV, Lei WL. Differential morphology of pyramidal tract-type and intratelencephalically projecting-type corticostriatal neurons and their intrastriatal terminals in rats. J. Comp. Neurol. 2003; 457:420–440. [PubMed: 12561080]

Reiner A, Lafferty DC, Wang HB, Del Mar N, Deng YP. The group 2 metabotropic glutamate receptor agonist LY379268 rescues neuronal, neurochemical and motor abnormalities in R6/2 Huntington's disease mice. Neurobiol. Dis. 2012a; 47:75–91. [PubMed: 22472187]

Reiner A, Wang HB, Del Mar N, Sakata K, Yoo W, Deng YP. BDNF may play a differential role in the protective effect of the mGluR2/3 agonist LY379268 on striatal projection neurons in R6/2 Huntington's disease mice. Brain Res. 2012b; 1473:161–172. [PubMed: 22820300]

Richfield EK, Maguire-Zeiss KA, Vonkeman HE, Voorn P. Preferential loss of preproenkephalin versus preprotachykinin neurons from the striatum of Huntington’s disease patients. Ann. Neurol. 1995; 38:852–861. [PubMed: 8526457]

Ridler TW, Calvard S. Picture thresholding using an iterative selection method. IEEE Transactions on Systems, Man and Cybernetics. 1978; 8:630–632.

Rising AC, Xu J, Carlson A, Napoli VV, Denovan-Wright EM, Mandel RJ. Longitudinal behavioral, cross-sectional transcriptional and histopathological characterization of a knock-in mouse model of Huntington's disease with 140 CAG repeats. Exp. Neurol. 2011; 228:173–182. [PubMed: 21192926]

Rosas HD, Hevelone ND, Zaleta AK, Greve DN, Salat DH, Fischl B. Regional cortical thinning in preclinical Huntington disease and its relationship to cognition. Neurology. 2005; 65:745–747. [PubMed: 16157910]

Rosas HD, Koroshetz WJ, Chen YI, Skeuse C, Vangel M, Cudkowicz ME, Caplan K, Marek K, Seidman LJ, Makris N, Jenkins BG, Goldstein JM. Evidence for more widespread cerebral pathology in early HD: an MRI-based morphometric analysis. Neurology. 2003; 60:1615–1620. [PubMed: 12771251]

Rosas HD, Tuch DS, Hevelone ND, Zaleta AK, Vangel M, Hersch SM, Salat DH. Diffusion tensor imaging in presymptomatic and early Huntington's disease: Selective white matter pathology and its relationship to clinical measures. Mov. Disord. 2006; 21:1317–1325. [PubMed: 16755582]

Rupp J, Blekher T, Jackson J, Beristain X, Marshall J, Hui S, Wojcieszek J, Foroud T. Progression in prediagnostic Huntington disease. J. Neurol. Neurosurg. Psychiatry. 2010; 81:379–384. [PubMed: 19726414]

Salin P, Kachidian P. Thalamo-striatal deafferentation affects preproenkephalin but not preprotachykinin gene expression in the rat striatum. Brain Res. Mol. Brain Res. 1998; 57:257–265. [PubMed: 9675424]

Selemon LD, Rajkowska G, Goldman-Rakic PS. Evidence for progression in frontal cortical pathology in late-stage Huntington's disease. J. Comp. Neurol. 2004; 468:190–204. [PubMed: 14648679]

Siemers E, Foroud T, Bill DJ, Sorbel J, Norton JA Jr, Hodes ME, Niebler G, Conneally PM, Christian JC. Motor changes in presymptomatic Huntington disease gene carriers. Arch. Neurol. 1996; 53:487–492. [PubMed: 8660148]

Singaraja RR, Huang K, Sanders SS, Milnerwood AJ, Hines R, Lerch JP, Franciosi S, Drisdel RC, Vaid K, Young FB, Doty C, Wan J, Bissada N, Henkelman RM, Green WN, Davis NG, Raymond LA, Hayden MR. Altered palmitoylation and neuropathological deficits in mice lacking HIP14. Hum. Mol. Genet. 2011; 20:3899–3909. [PubMed: 21775500]

Smith Y, Raju D, Nanda B, Pare JF, Galvan A, Wichmann T. The thalamostriatal systems: anatomical and functional organization in normal and parkinsonian states. Brain Res. Bull. 2009; 78:60–68. [PubMed: 18805468]

Smith Y, Raju DV, Pare JP, Sidibe M. The thalamostriatal system: a highly specific network of the basal ganglia circuitry. Trends Neurosci. 2004; 27:520–527. [PubMed: 15331233]

Smith Y, Surmeier DJ, Redgrave P, Kimura M. Thalamic contributions to Basal Ganglia-related behavioral switching and reinforcement. J. Neurosci. 2011; 31:16102–16106. [PubMed: 22072662]

Sotrel A, Paskevich PA, Kiely DK, Bird ED, Williams RS, Myers RH. Morphometric analysis of the prefrontal cortex in Huntington's disease. Neurology. 1991; 41:1117–1123. [PubMed: 1829794]

Squitieri F, Cannella M, Simonelli M, Sassone J, Martino T, Venditti E, Ciammola A, Colonnese C, Frati L, Ciarmiello A. Distinct Brain Volume Changes Correlating with Clinical Stage, Disease Progression Rate, Mutation Size, and Age at Onset Prediction as Early Biomarkers of Brain Atrophy in Huntington's Disease. CNS Neurosci. Ther. 2009; 15:1–11. [PubMed: 19228174]

Strand AD, Baquet ZC, Aragaki AK, Holmans P, Yang L, Cleren C, Beal MF, Jones L, Kooperberg C, Olson JM, Jones KR. Expression profiling of Huntington's disease models suggests that brain-derived neurotrophic factor depletion plays a major role in striatal degeneration. J. Neurosci. 2007; 27:11758–11768. [PubMed: 17959817]

Sun Z, Xie J, Reiner A. The differential vulnerability of striatal projection neurons in 3-nitropropionic acid-treated rats does not match that typical of adult-onset Huntington's disease. Exp. Neurol. 2002; 176:55–65. [PubMed: 12093082]

Tabrizi SJ, Scahill RI, Durr A, Roos RA, Leavitt BR, Jones R, Landwehrmeyer GB, Fox NC, Johnson H, Hicks SL, Kennard C, Craufurd D, Frost C, Langbehn DR, Reilmann R, Stout JC. TRACK-HD Investigators. Biological and clinical changes in premanifest and early stage Huntington's disease in the TRACK-HD study: the 12-month longitudinal analysis. Lancet Neurol. 2011; 10:31–42. [PubMed: 21130037]

Turner TH, Goldstein J, Hamilton JM, Jacobson M, Pirogovsky E, Peavy G, Corey-Bloom J. Motor abnormalities in premanifest persons with Huntington's disease: the PREDICT-HD study. J. Mot. Behav. 2011; 43:295–302. [PubMed: 21774606]

van den Bogaard SJ, Dumas EM, Ferrarini L, Milles J, van Buchem MA, van der Grond J, Roos RA. Shape analysis of subcortical nuclei in Huntington's disease, global versus local atrophy--results from the TRACK-HD study. J. Neurol. Sci. 2011; 307:60–68. [PubMed: 21624624]

Varoqui H, Schäfer MKH, Zhu H, Weihe E, Erickson JD. Identification of the differentiation-associated Na+/PI transporter as a novel vesicular glutamate transporter expressed in a distinct set of glutamatergic synapses. J. Neurosci. 2002; 22:142–155. [PubMed: 11756497]

Vonsattel JP. Huntington disease models and human neuropathology: similarities and differences. Acta Neuropathol. 2008; 115:55–69. [PubMed: 17978822]

Vonsattel JP, DiFiglia M. Neuropathological classification of Huntington's disease. J. Neuropathol. Exp. Neurol. 1998; 57:369–384. [PubMed: 9596408]

Vonsattel JP, Myers RH, Stevens TJ, Ferrante RJ, Bird ED, Richardson EP Jr. Neuropathological classification of Huntington's disease. J. Neuropathol. Exp. Neurol. 1985; 44:559–577. [PubMed: 2932539]

Wang HB, Deng YP, Reiner A. In situ hybridization histochemical and immunohistochemical evidence that striatal projection neurons co-containing substance P and enkephalin are overrepresented in the striosomal compartment of striatum in rats. Neurosci. Lett. 2007; 425:195–199. [PubMed: 17868995]

Wässle H, Regus-Leidig H, Haverkamp S. Expression of the vesicular glutamate transporter vGluT2 in a subset of cones of the mouse retina. J. Comp. Neurol. 2006; 496:544–555. [PubMed: 16572432]

Wilson CJ. Morphology and synaptic connections of crossed corticostriatal neurons in the rat. J. Comp. Neurol. 1987; 263:567–580. [PubMed: 2822779]

Wilson, CJ. Dendritic morphology, inward rectification and the functional properties of neostriatal neurons. In: McKenna, T., et al., editors. Single neuron computation. Academic Press; 1992. p. 141-171.

Wilson CJ, Chang HT, Kitai ST. Origins of postsynaptic potentials evoked in identified neostriatal neurons by stimulation in substantia nigra. Exp. Brain Res. 1982; 45:157–167. [PubMed: 7056322]

Wilson CJ, Groves PM, Kitai ST, Linder JC. Three-dimensional structure of dendritic spines in the rat neostriatum. J Neurosci. 1983; 3:383–388. [PubMed: 6822869]

Wolf RC, Grön G, Sambataro F, Vasic N, Wolf ND, Thomann PA, Saft C, Landwehrmeyer GB, Orth M. Brain activation and functional connectivity in premanifest Huntington's disease during states of intrinsic and phasic alertness. Human Brain Mapping. 2012; 33:2161–2173. [PubMed: 22887827]

Wolf RC, Sambataro F, Vasic N, Schönfeldt-Lecuona C, Ecker D, Landwehrmeyer B. Aberrant connectivity of lateral prefrontal networks in presymptomatic Huntington's disease. Exp Neurol. 2008a; 213:137–144. [PubMed: 18588876]

Wolf RC, Sambataro F, Vasic N, Schönfeldt-Lecuona C, Ecker D, Landwehrmeyer B. Altered frontostriatal coupling in pre-manifest Huntington's disease: effects of increasing cognitive load. Eur. J. Neurol. 2008b; 15:1180–1190. [PubMed: 18754766]

Wright AK, Norrie L, Ingham CA, Hutton EA, Arbuthnott GW. Double anterograde tracing of outputs from adjacent "barrel columns" of rat somatosensory cortex. Neostriatal projection patterns and terminal ultrastructure. Neuroscience. 1999; 88:119–133. [PubMed: 10051194]

Wright AK, Ramanathan S, Arbuthnott GW. Identification of the source of the bilateral projection system from cortex to somatosensory neostriatum and an exploration of its physiological actions. Neuroscience. 2001; 103:87–96. [PubMed: 11311789]

Highlights

- Loss of excitatory input to striatum precedes striatal neuron loss in Q140 HD mice
- Loss of excitatory drive to striatum may explain motor deficits in premanifest HD
- An early deficiency in thalamic input to striatum occurs in Q140 HD mice
- Thalamostriatal connectivity may never form correctly in HD

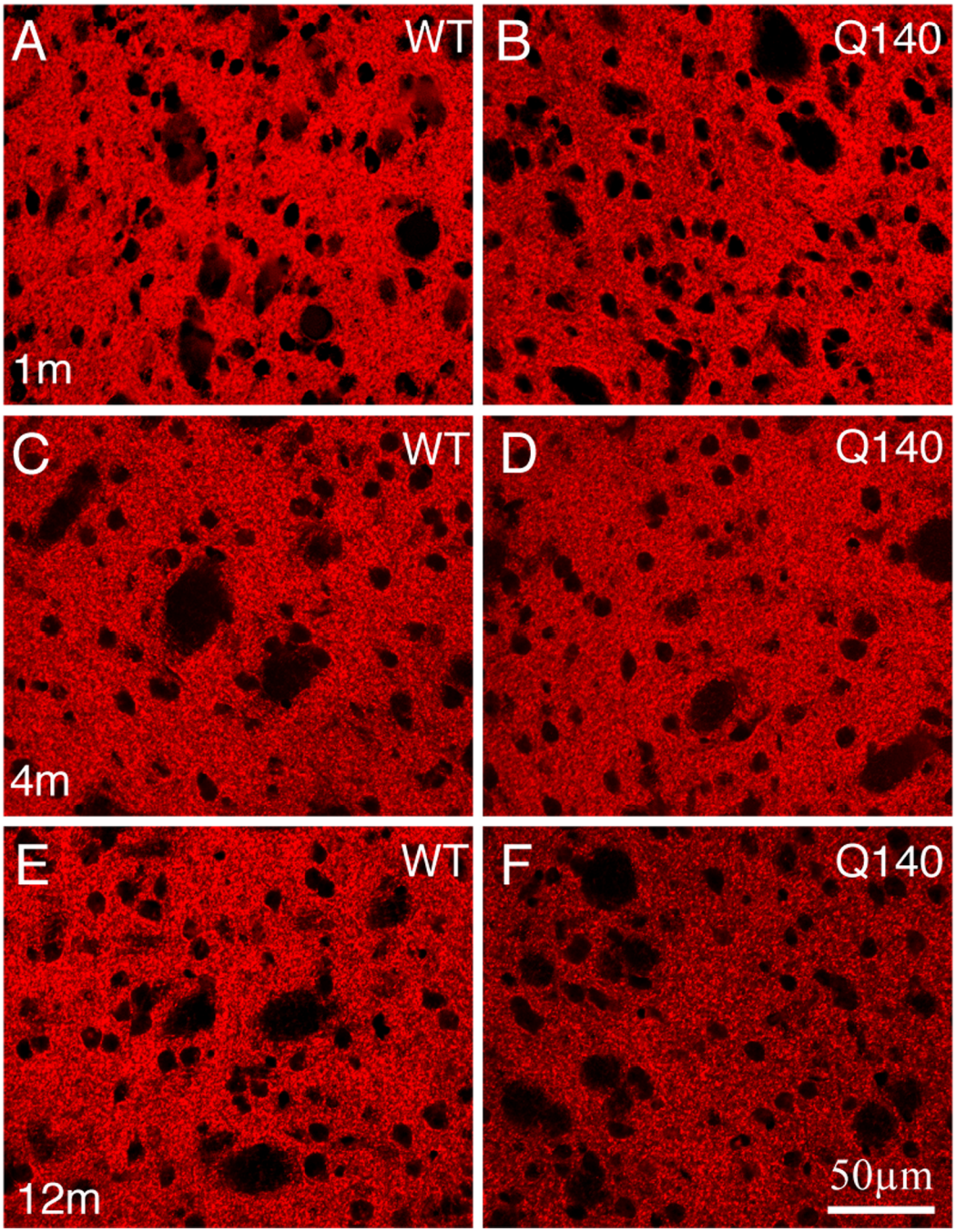

Figure 1.
CLSM views of immunofluorescence labeling for VGLUT1 corticostriatal terminals in striatum of 1 month- (A, B), 4 month- (C, D), and 12 month-old (E, F) wildtype (A, C, E) and heterozygous Q140 Huntington's disease knock-in (B, D, F) mice. All images are at the same magnification.

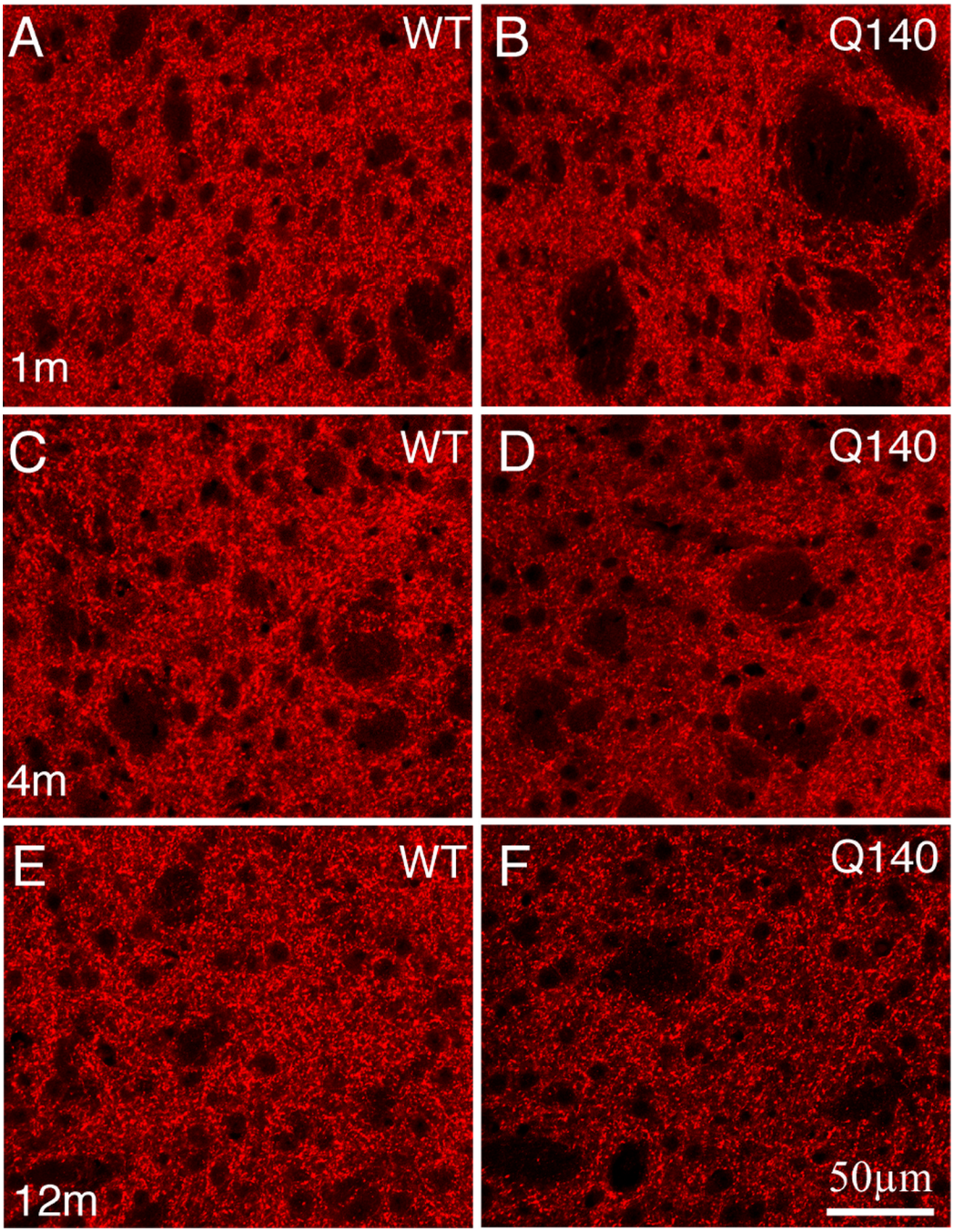

Figure 2.
CLSM views of immunofluorescence for VGLUT2 thalamostriatal terminals in striatum of 1 month- (A, B), 4 month- (C, D), and 12 month-old (E, F) wildtype (A, C, E) and heterozygous Q140 Huntington's disease knock-in (B, D, F) mice. All images are at the same magnification.

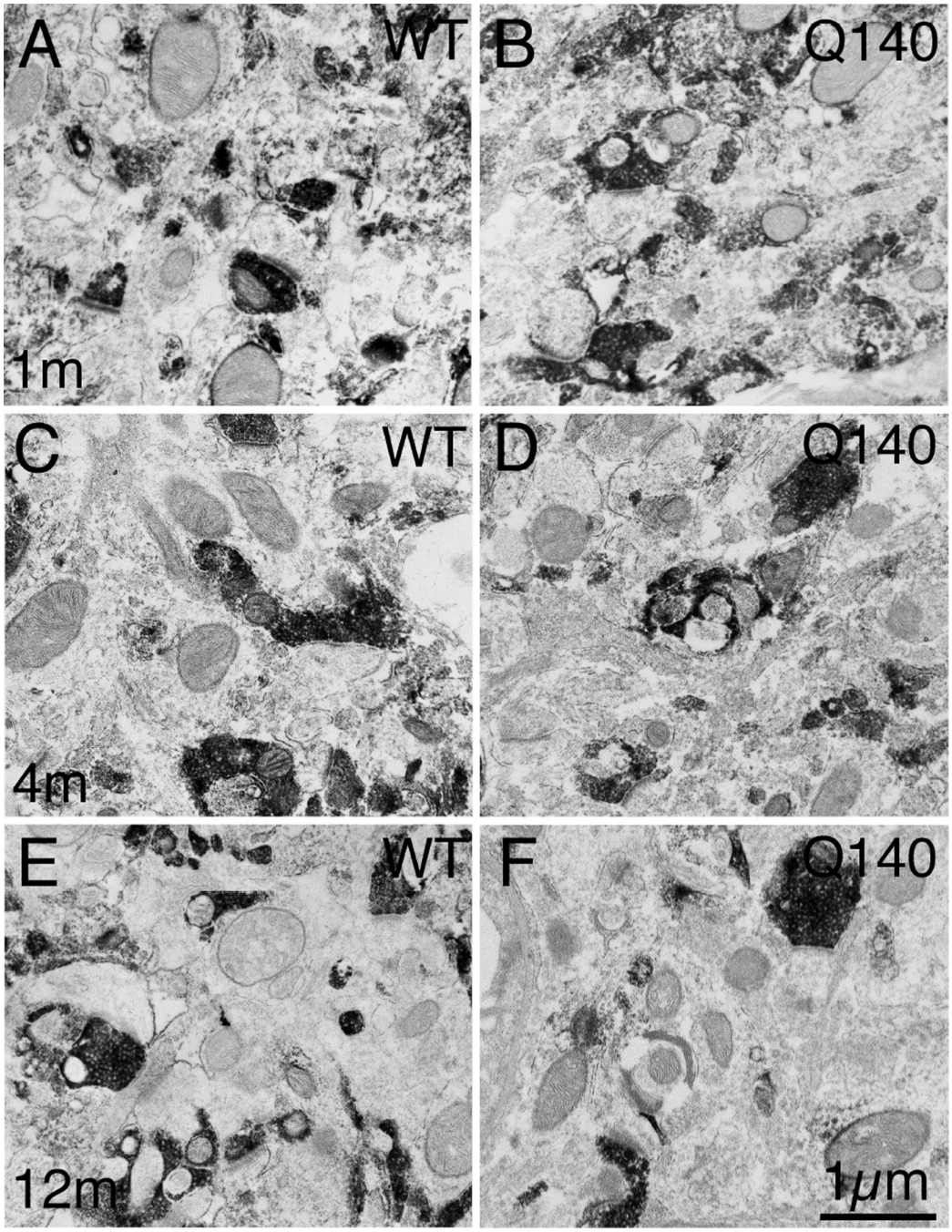

Figure 3.
EM images of VGLUT1+ immunolabeled synaptic terminals in striatum of 1 month- (A, B), 4 month- (C, D), and 12 month-old (E, F) wildtype (A, C, E) and heterozygous Q140 Huntington's disease knock-in (B, D, F) mice. The relatively low power views show many labeled terminals, and typify the decline in VGLUT1 terminals seen in Q140 mice at 12 months. All images are at the same magnification.

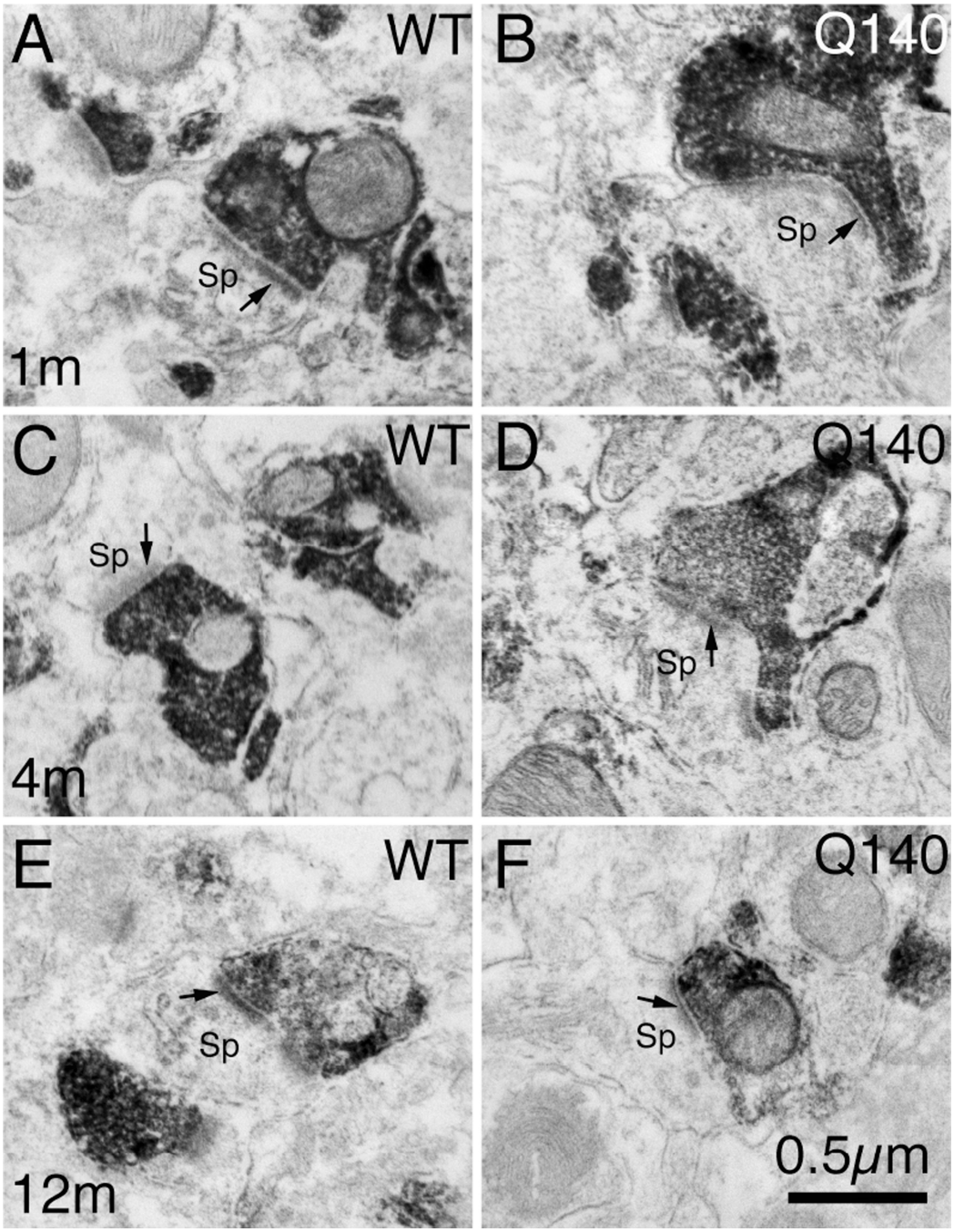

Figure 4.

Higher magnification EM images of VGLUT1+ immunolabeled synaptic terminals on spines of striatal projection neurons in striatum of 1 month- (A, B), 4 month- (C, D), and 12 month-old (E, F) wildtype (A, C, E) and heterozygous Q140 Huntington knock-in (B, D, F) mice. Spines (Sp) were recognizable by their small size, the presence of spine apparatus, and the absence of mitochondria and microtubules. All VGLUT1+ synaptic terminals formed asymmetric synaptic contacts, as recognizable by the thick postsynaptic density (PSD, arrow). All images are at the same magnification.

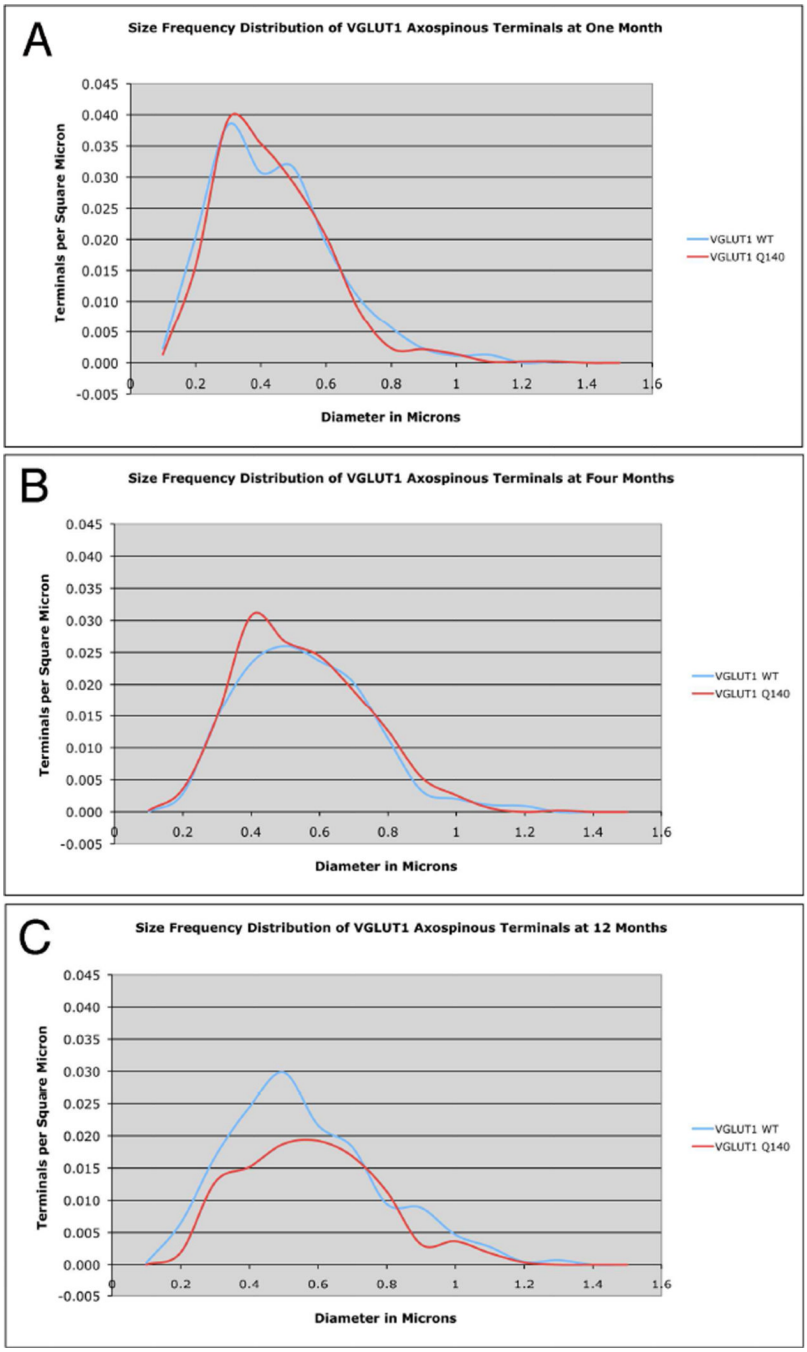

Figure 5.

Graphs showing the size frequency distributions for VGLUT1+ axospinous synaptic terminals in striatum of 1 month- (A), 4 month- (B), and 12 month-old (C) wildtype and heterozygous Q140 Huntington knock-in mice. Note that at 12 months a noteworthy shortfall in small terminals is evident in Q140 mice.

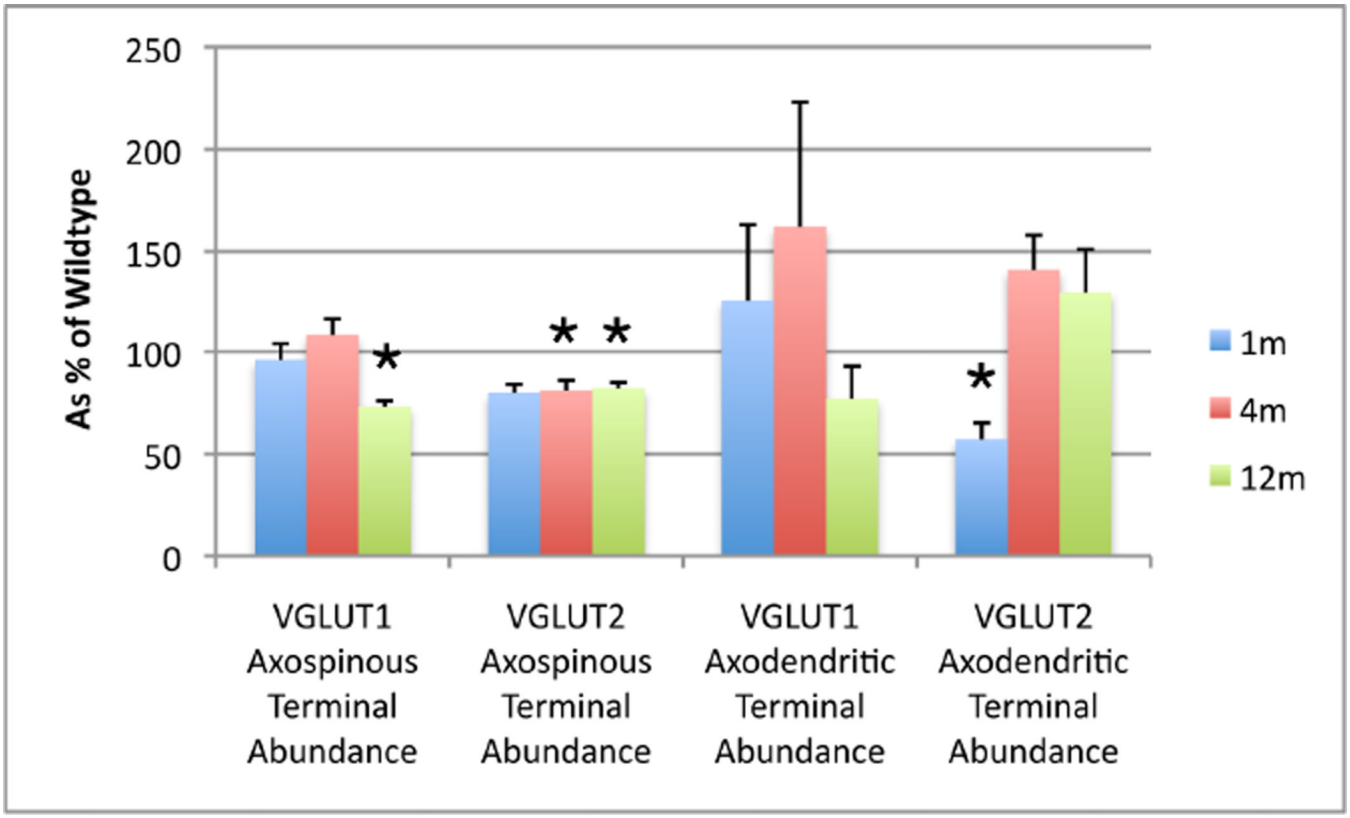

Figure 6.
Graph showing the abundance of axospinous and axodendritic VGLUT1 and VGLUT2 terminals in striatum from 1 month-, 4 month-, and 12 month-old heterozygous Q140 knock-in Huntington's disease mice as a percent of WT. * $p<0.05$, compared to wildtype, by parametric t-test for 12-month VGLUT1 axospinous, 4-month VGLUT2 axospinous, and 1-month VGLUT2 axodendritic terminals. The asterisk in the case of 12-month VGUT2 axospinous terminals reflects a significant difference between Q140 and WT for terminals in the 0.5–0.8 μm range, by a parametric t-test with Bonferroni correction for multiple comparisons.

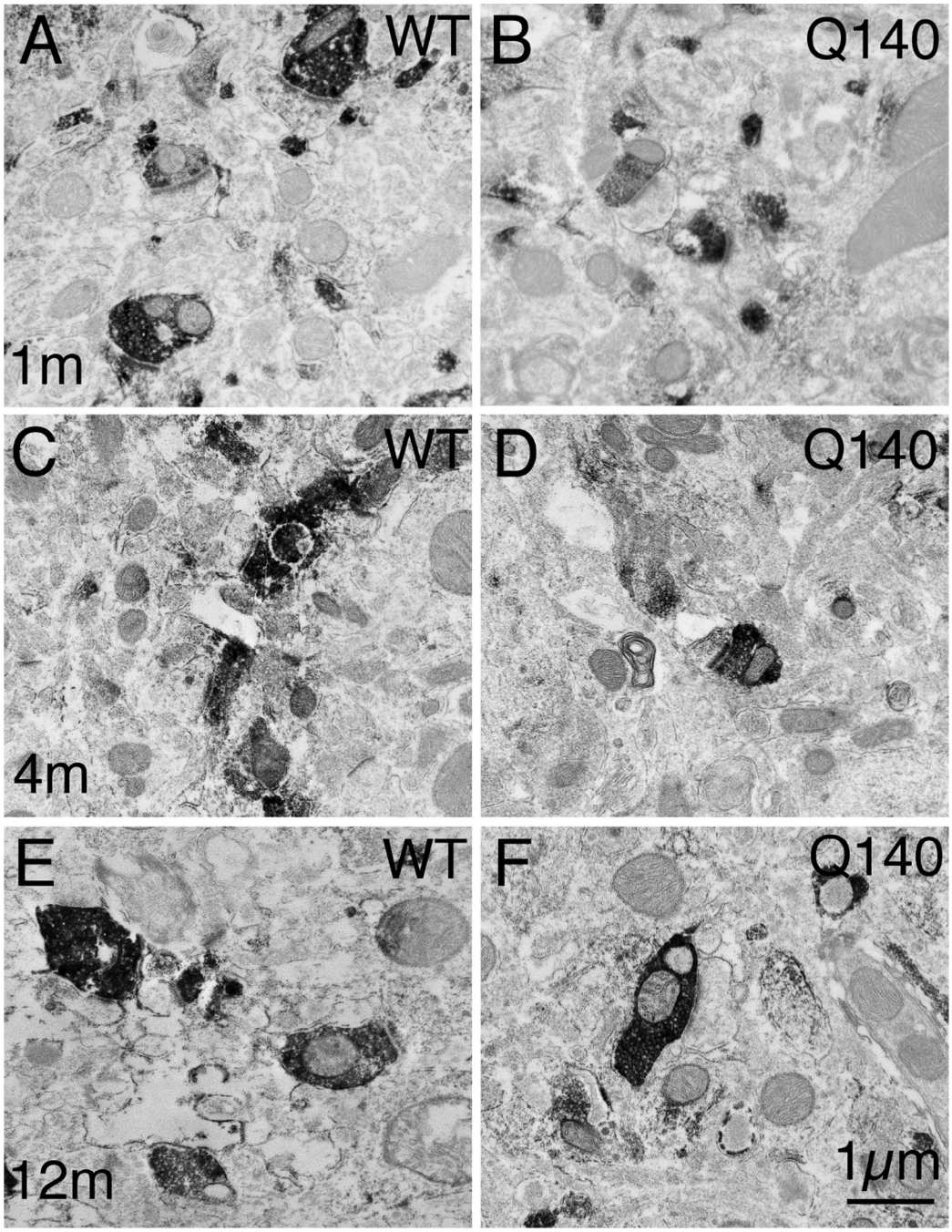

Figure 7.
EM images of VGLUT2+ immunolabeled synaptic terminals in striatum of 1 month- (A, B), 4 month- (C, D), and 12 month-old (E, F) wildtype (A, C, E) and heterozygous Q140 Huntington's disease knock-in (B, D, F) mice. The relatively low power views show many labeled terminals, and typify the shortfall in VGLUT2 terminals seen in Q140 mice at all ages. All images are at the same magnification.

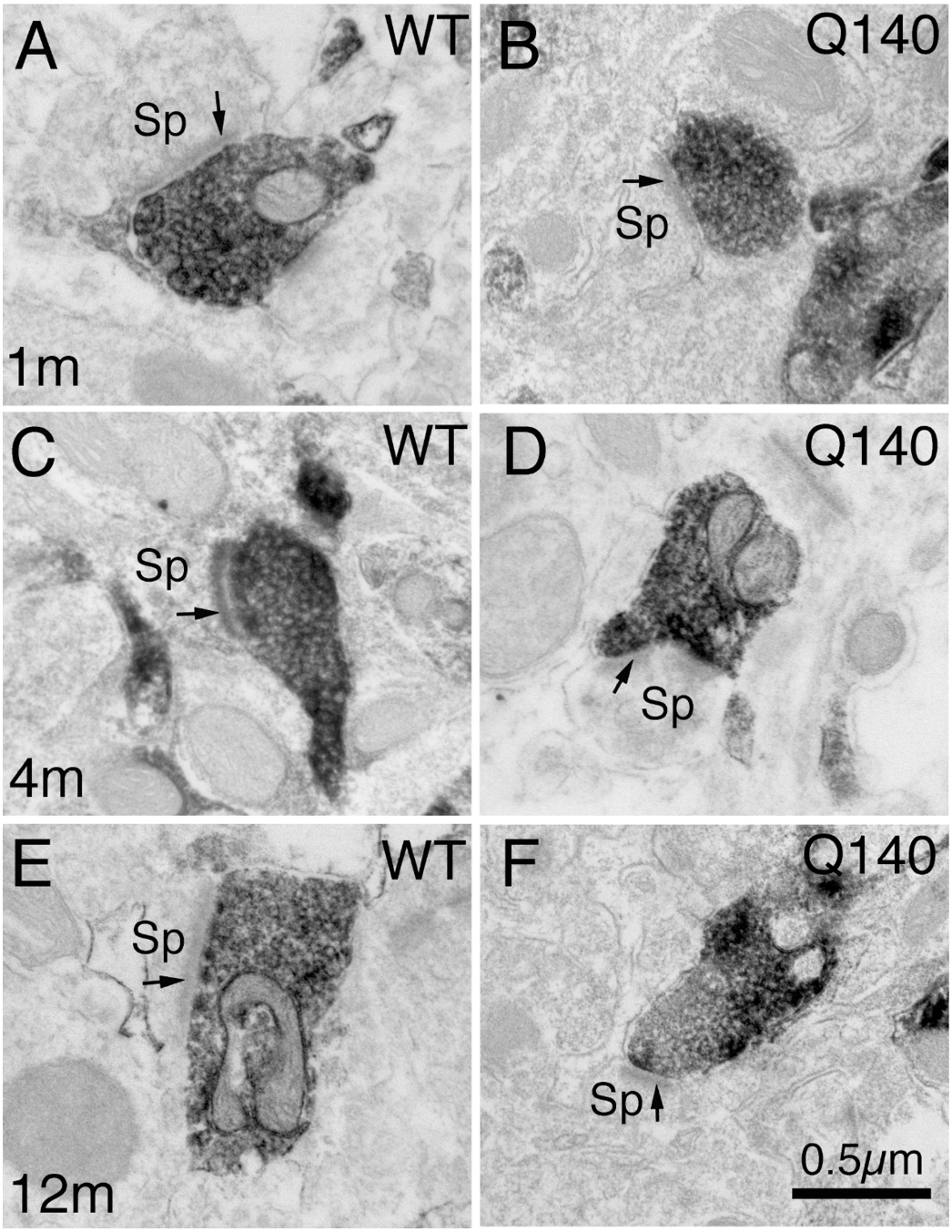

Figure 8.

Higher magnification EM images of VGLUT2+ immunolabeled synaptic terminals on spines of striatal projection neurons in striatum of 1 month- (A, B), 4 month- (C, D), and month-old (E, F) wildtype (A, C, E) and heterozygous Q140 Huntington's disease knock-in (B, D, F) mice. Spines (Sp) were recognizable by their small size, the presence of spine apparatus, and the absence of mitochondria and microtubules. All VGLUT2+ synaptic terminals formed asymmetric synaptic contacts, as recognizable by the thick postsynaptic density (PSD, arrow). All images are at the same magnification.

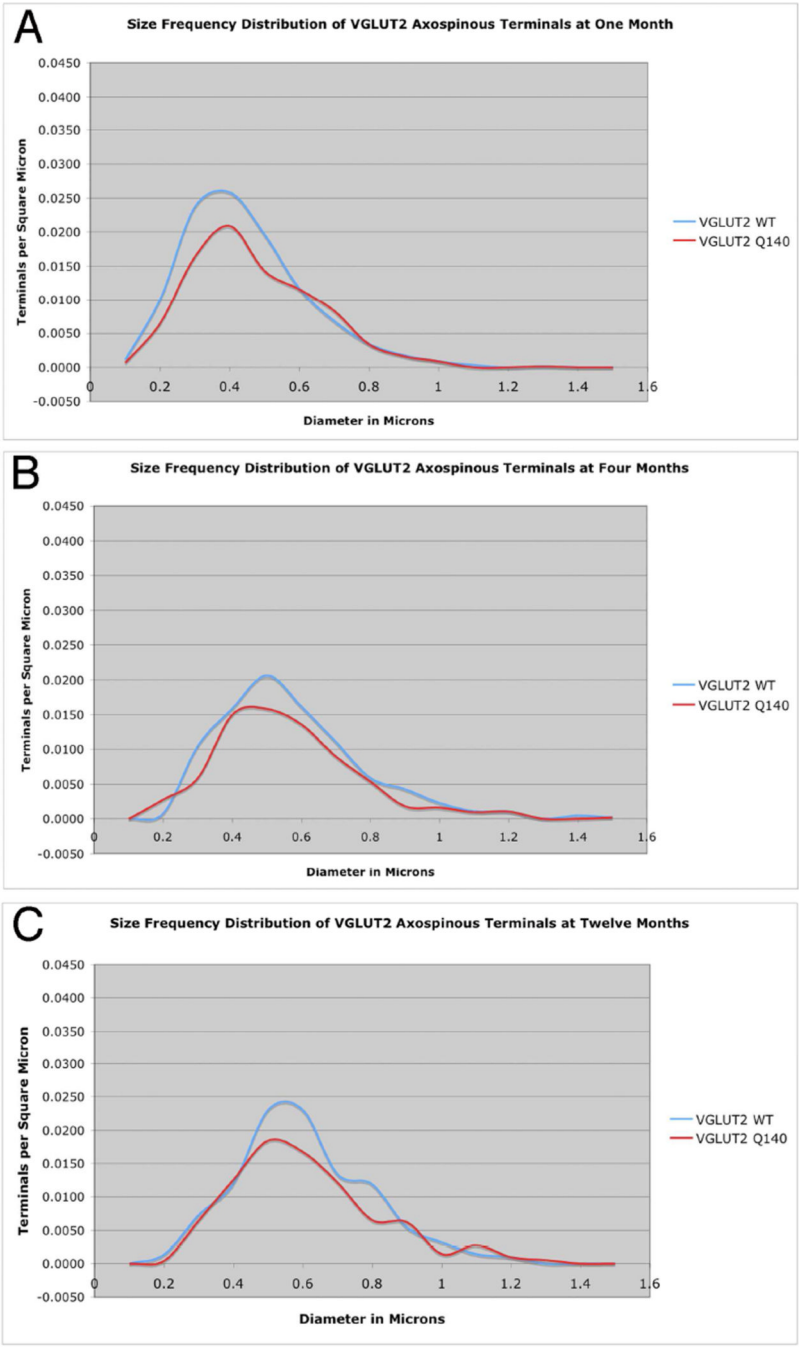

Figure 9.

Graphs showing the size frequency distributions for VGLUT2+ axospinous synaptic terminals in striatum of 1 month- (A), 4 month- (B), and 12 month-old (C) wildtype and heterozygous Q140 Huntington knock-in mice. Note that a shortfall in small terminals was found in Q140 mice at 1, 4 months and 12 months.

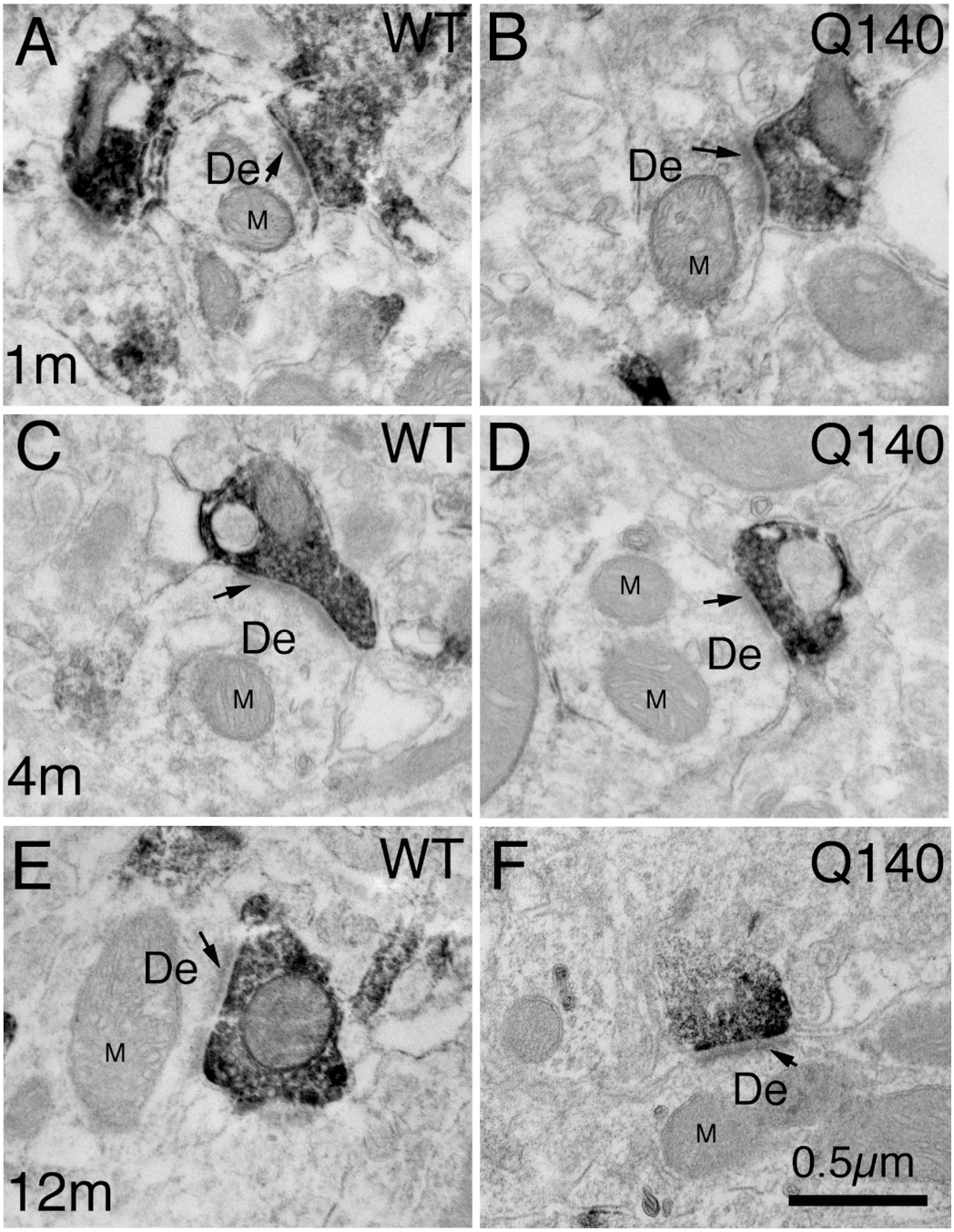

Figure 10.

High magnification EM images of VGLUT2+ immunolabeled synaptic terminals on dendrites of striatal neurons from 1 month- (A, B), 4 month- (C, D), and 12 month-old (E, F) wildtype (A, C, E) and heterozygous Q140 Huntington's disease knock-in (B, D, F) mice. Dendrites (De) were recognizable by their larger size, the presence of mitochondria (M) and microtubules, and the absence of spine apparatus. Arrow indicates postsynaptic density (PSD). All images are at the same magnification.

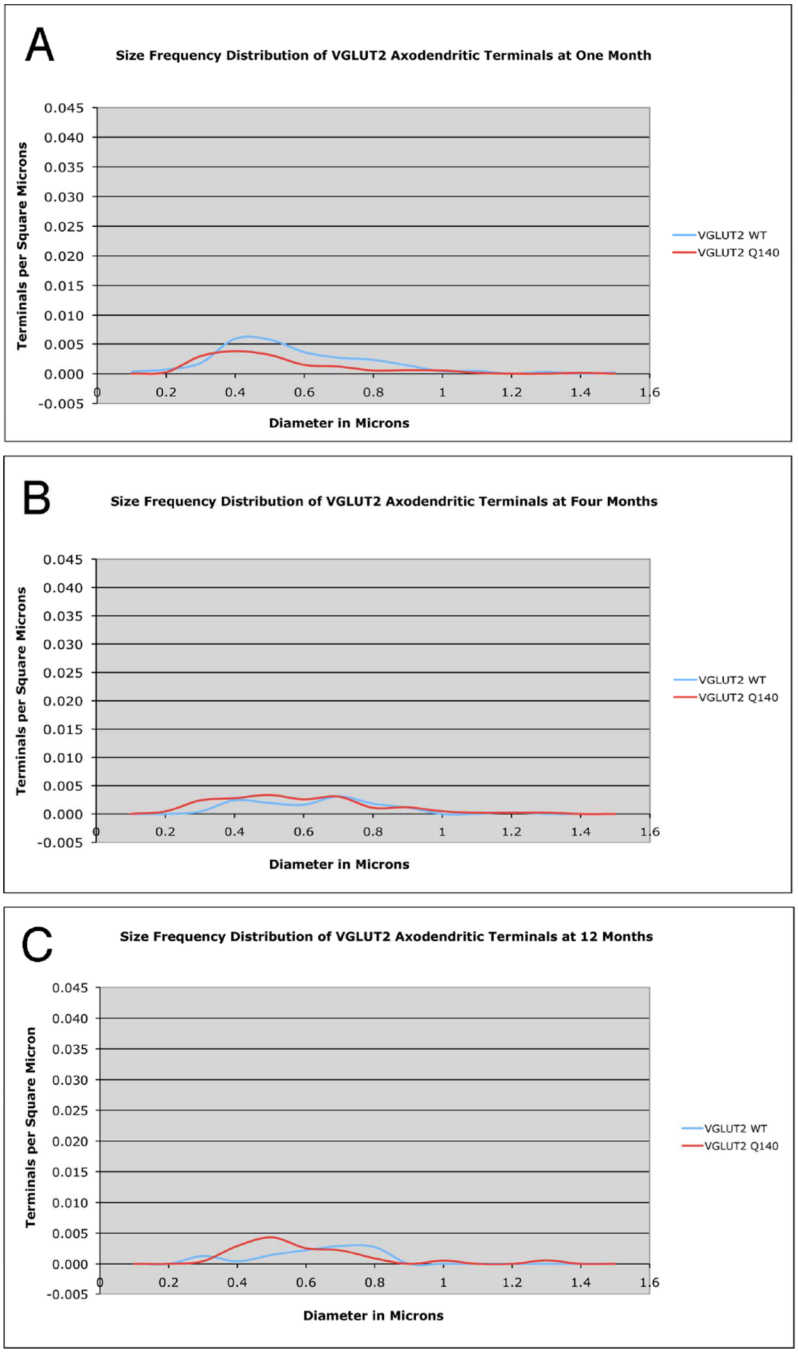

Figure 11.

Graphs showing the size frequency distributions for VGLUT2+ axodendritic synaptic terminals in striatum of 1 month- (A), 4 month- (B), and 12 month-old (C) wildtype and heterozygous Q140 Huntington's disease knock-in mice. Note that a shortfall in large terminals was found in Q140 mice at 1 month, but not at 4 months. At 12 months, a shortfall was again seen in Q140 mice, specifically for large (0.8μm diameter) terminals.

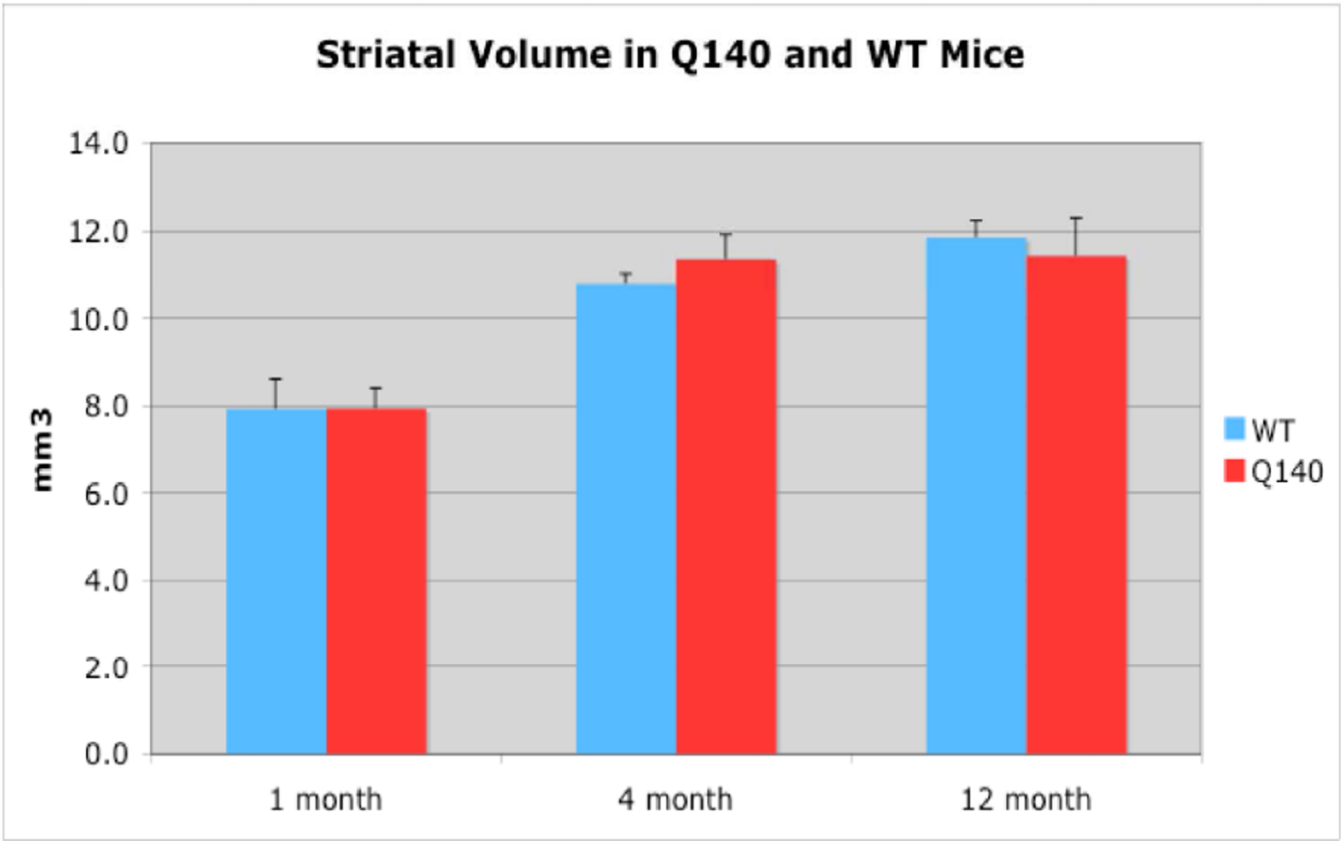

Figure 12.
Graphs showing quantitative striatal volumetry data from 1 month-, 4 month-, and 12 month-old wildtype and heterozygous Q140 Huntington's disease knock-in mice. Note that striatal volume in Q140 mice does not differ from that in WT at any of the ages examined.

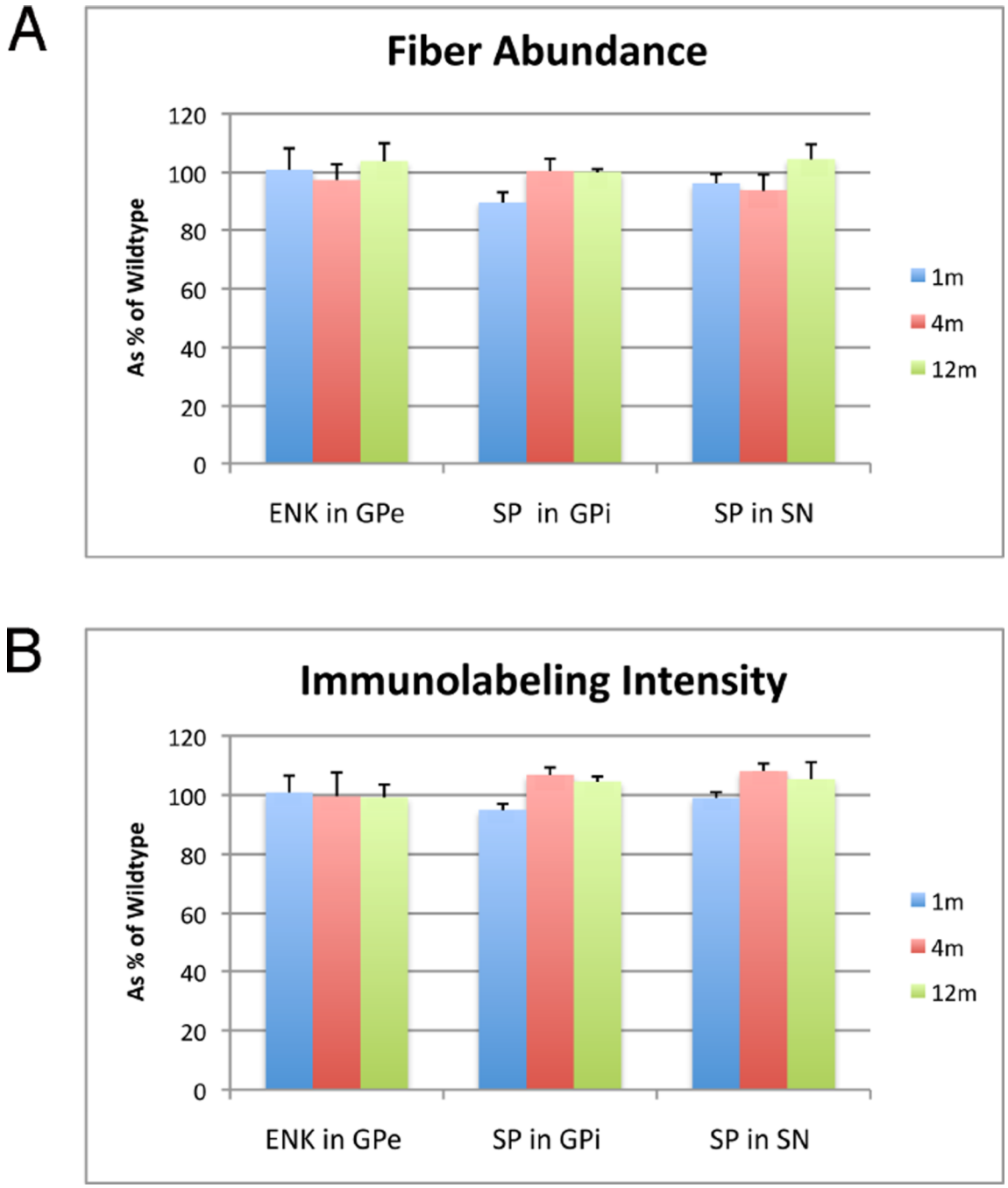

Figure 13.

Graphs showing abundance (A) and intensity (B) of substance P-immunolabeling in striatal terminals in GPi and SN, and ENK-immunolabeling in striatal terminals in GPe of 1 month-, 4 month-, and 12 month-old wildtype and heterozygous Q140 Huntington's knock-in mice, presented in all cases as a percent of WT mice (±SEM). Note that abundance and labeling intensity for these three fiber types does not differ significantly between Q140 and WT at any of the three ages examined, by a parametric t-test.

Table 1

The abundance of VGLUT1 and VGLUT2 immunolabeling in striatum of heterozygous Q140 knock-in Huntington disease mice relative to WT mice, as determine by quantification of immunofluourescence labeling in CLSM images, is separately shown for VGLUT1 and VGLUT2. The columns show the number of Q140 and WT animals analyzed per age group, the mean CAG repeat length for Q140 mice per age group, and the relative intensity of overall striatal labeling, the relative intensity of labeling in VGLUT+ fibers, and the relative abundance of VGLUT fibers. Parametric t-tests were used to evaluate differences between WT and Q140 mice within each of the three age groups examined for each of the parameters measured.

Age	**Number of Animals**	**Q140 CAG**	**VGLUT1 Intensity - Entire Striatum**	**VGLUT1 Intensity - Striatal Fibers**	**Striatal Area Occupied by VGLUT1 Fibers**	**Results Shown as**
1 month	7 WT, 8 Q140	127.8	96.1% ±10.8	97.1% 7.9	100.8% ±7.5	% of WT
4 month	5 WT, 5 Q140	128.6	93.0% ±8.9	93.6% ±9.2	95.6% 2.7	% of WT
12 month	5 WT, 5 Q140	135.0	**78.0% ±7.0** *	***82.4% ±6.4***	78.2% ±4.5	% of WT
Age	Number of Animals	Q140 CAG	VGLUT2 Intensity - Entire Striatum	VGLUT2 Intensity - Striatal Fibers	Striatal Area Occupied by VGLUT2 Fibers	Results Shown as
1 month	7 WT, 8 Q140	127.8	111.9±9.5%	105.8±6.1%	101.7±4.8%	% of WT
4 month	5 WT, 5 Q140	128.6	107.4±9.4%	110.3±8.7%	90.4±4.6%	% of WT
12 month	5 WT, 5 Q140	135.0	**84.7±5.0%** *	***80.3±2.1%***	**77.6±5.7%** *	% of WT

Mean ± Standard Deviation,

Bold & * = $p<0.05$,

Bold & Ital = $p<0.055$.

Table 2

The size and abundance of VGLUT1+ and VGLUT2+ synaptic terminals in striatum of WT and heterozygous Q140 knock-in Huntington disease mice, as determined by quantification of EM images, are shown. The columns show the number of Q140 and WT animals analyzed per age group, the mean CAG repeat length for Q140 mice per age group, and the size or abundance of VGLUT1 axospinous, VGLUT2 axospinous, VGLUT1 axodendritic, and VGLUT2 axodendritic terminals. Parametric t-tests were used to evaluate differences between WT and Q140 mice within each of the three age groups examined for each of the parameters measured, with the exceptions that a Mann-Whitney U nonparametric t-test was performed for VGLUT1 axospinous and axodendritic terminal size at one month, for VGLUT1 axospinous terminal spatial frequency at one month, and for VGLUT2 axospinous terminal spatial frequency at 1 and 12 months, since they were not normally distributed.

Age	**Animals**	**Q140 CAG**	**VGLUT1 Axospinous Terminal Diameter**	**VGLUT2 Axospinous Terminal Diameter**	**VGLUT1 Axodendritic Terminal Diameter**	**VGLUT2 Axodendritic Terminal Diameter**	**Results Shown in**
1 month	7 WT, 7 Q140	126.8	WT=0.492 Q140=0.485	WT=0.514 Q140=0.521	WT=0.565 Q140=0.572	WT=0.615 Q140=0.566	in μm
4 month	5 WT, 5 Q140	128.6	WT=0.604 Q140=0.593	WT=0.623 Q140=0.603	WT=0.644 Q140=0.661	WT=0.671 Q140=0.641	in μm
12 month	5 WT, 5 Q140	135.0	WT=0.608 Q140=0.628	WT=0.656 Q140=0.660	WT=0.902 Q140=0.696	WT=0.672 Q140=0.649	in μm
Age	**Animals**	**Q140 CAG**	**VGLUT1 Axospinous Terminal Abundance**	**VGLUT2 Axospinous Terminal Abundance**	**VGLUT1 Axodendritic Terminal Abundance**	**VGLUT2 Axodendritic Terminal Abundance**	**Results Shown as**
1 month	7 WT, 7 Q140	126.8	WT=0.1520±0.0150 Q140=0.1461±0.0132	WT=0.1055±0.0120 Q140=0.0846±0.0065	WT=0.0114±0.0039 Q140=0.0144±0.0046	**WT=0.0260±0.0030** **Q140=0.0149±0.0023**	per μm^2
4 month	5 WT, 5 Q140	128.6	WT=0.1295±0.0114 Q140=0.1402±0.0115	**WT=0.0902±0.0061** **Q140=0.0730±0.0065**	WT=0.0059±0.0020 Q140=0.0096±0.0041	WT=0.0127±0.0021 Q140=0.0180±0.0024	per μm^2
12 month	5 WT, 5 Q140	135.0	**WT=0.1444±0.0077** **Q140=0.1050±0.0055**	***WT=0.1030±0.0105*** ***Q140=0.0851±0.0033***	WT=0.0079±0.0033 Q140=0.0061±0.0014	WT=0.0111±0.0014 Q140=0.0144±0.0026	per μm^2

Mean ± Standard Deviation,

Bold = $p<0.05$,

Bold & ital = 0.5–0.8 μm range significant at $p<0.05$ with Bonferroni correction for multiple comparisons

Table 3

The table expresses the abundance of each VGLUT terminal type in striatum for WT and heterozygous Q140 mice relative to all VGLUT terminal types detected in striatum. The columns show the number of Q140 and WT animals analyzed per age group, the mean CAG repeat length for Q140 mice per age group, and percent of total VGLUT terminals constituted by VGLUT1 axospinous, VGLUT2 axospinous, VGLUT1 axodendritic, and VGLUT2 axodendritic synaptic terminals in striatum.

Q140 Age	Animals	Q140 CAG	VGLUT1 Axospinous Terminal Abundance	VGLUT2 Axospinous Terminal Abundance	VGLUT1 Axodendritic Terminal Abundance	VGLUT2 Axodendritic Terminal Abundance	Results Shown as
1 month	7 WT, 7 Q140	126.8	WT=51.55% Q140=55.97%	WT=35.53% Q140=32.97%	WT=3.92% Q140=5.37%	WT=9.00% Q140=5.68%	As % all VGLUT
4 month	5 WT, 5 Q140	128.6	WT=54.21% Q140=58.02%	WT=37.92% Q140=30.63%	WT=2.54% Q140=3.80%	WT=5.33% Q140=7.55%	As % all VGLUT
12 month	5 WT, 5 Q140	135.0	WT=54.49% Q140=49.80%	WT=38.39% Q140=40.44%	WT=2.86% Q140=2.85%	WT=4.26% Q140=6.91%	As % all VGLUT